Universidade de Aveiro Departamento de Química
2018

José Nuno Magalhães Silvares

Desenvolvimento e aplicação de polioxometalatos funcionalizados como marcadores fluorescentes em biossensores

Development and application of functionalized polyoxometalates as fluorescent-tags in biosensing applications

Universidade de Aveiro Departamento de Química
2018

José Nuno Magalhães Silvares

Desenvolvimento e aplicação de polioxometalatos funcionalizados como marcadores fluorescentes em biossensores

Development and application of functionalized polyoxometalates as fluorescent-tags in biosensing applications

Dissertação apresentada à Universidade de Aveiro para cumprimento dos requisitos necessários à obtenção do grau de Mestre em Biotecnologia, ramo Molecular, realizada sob orientação científica da Doutora Filipa Lourosa Sousa, Investigadora Auxiliar do Departamento de Química da Universidade de Aveiro e do Doutor Duarte Miguel de França Teixeira dos Prazeres, Professor Catedrático do Departamento de Bioengenharia do Instituto Superior Técnico

Trabalho financiado pela Bolsa de Investigação BI/IU89/7529/2016 e enquadrado no projeto ThermoPoms project P2020-PTDC-QEQ-QIN-5975-2014 e CICECO-Aveiro Institute of Materials, POCI-01-0145-FEDER-007679 (FCT Ref. UID /CTM /50011/2013), financiados por fundos nacionais pela FCT/MEC e cofinanciado pelo FEDER sob acordo de parceria PT2020

acknowledgements

Firstly, I would like to thank my thesis supervisor Doctor Filipa Sousa of CICECO – Aveiro Institute of Materials at University of Aveiro who took a chance on me and trusted me to develop this project. I would also like to thank Professor Miguel Prazeres of Institute for Bioengineering and Biosciences at Instituto Superior Técnico for his expertise and allowing me to join his highly qualified research group.

I would also like to acknowledge my colleagues at IST who helped me during my stay in Lisbon, particularly PhD student Rui Silva that has been my greatest advisor, and my colleagues at University of Aveiro. To Doctor Pedro Paulo, I must thank for allowing me to use his spectrofluorometer and for all the very enriching and teaching conversations.

I must express my very profound gratitude to the people without whom I would never be where I am at, my parents, my brother and my godmother, for providing with unfailing support and encouragement through all this process. I would also wish to mention the people who became my chosen family. To João Costa, João Cabral and Miguel Costa, I must thank for the life-long friendship that is one of the achievements I am most grateful for in life. For the companionship, patience and always challenging me to be better over the past 5 years, I must thank Adriana Pais, Ana Celina, João Santos, João Trigo, Joshua Anjos and Sara Oliveira.

Finally, these acknowledgements would not be completed without referring to my teammates and my club (Alavarium Andebol Clube de Aveiro) that have taught me that sacrifices are inevitable to fulfil our personal goals, but it will all be worthy in the end.

o júri

presidente

Professora Doutora Luísa Alexandra Seuanes Serafim Martins Leal
Professora Auxiliar do Departamento de Química da Universidade de Aveiro

vogais

Doutor Marcelino Miguel Guedes de Jesus Oliveira
Investigador Auxiliar do Departamento de Biologia da Universidade de Aveiro

Doutora Filipa Lourosa Sousa
Investigadora Auxiliar do Departamento de Química da Universidade de Aveiro

Palavras-chave Polioxometalatos, Lantanídeos, Luminescência, Biossensores, ADN, Anticorpos, Celulose

Resumo

Esta tese teve como objetivo o desenvolvimento de sensores de papel fluorescentes, tirando partido das propriedades óticas de lantanopolioxometalatos para obter resultados de forma rápida, usando uma lâmpada de UV, portátil e barata. Os polioxometalatos (POMs) selecionados foram do tipo Keggin monolacunar e $[Ln(W_5O_{18})_2]^{9-}$ contendo európio. Nanopartículas do tipo núcleo-coroa (~24 nm), com núcleo do anião $[Ln(W_5O_{18})_2]^{9-}$ encapsulado em sílica, foram sintetizadas e sucessivamente funcionalizadas de forma a maximizar a afinidade para os analitos de interesse.

No caso do anião $[EuPW_{11}O_{39}(H_2O)_2]^{4-}$ ($EuPW_{11}$), foi explorada uma estratégia mais direta para avaliar a potencial afinidade deste anião para interagir com uma sequência de ADN, recorrendo ao uso da espectroscopia de fluorescência. Avaliou-se o efeito da adição de ADN a soluções aquosas de $EuPW_{11}$ na intensidade das bandas de fluorescência correspondentes às três principais transições do catião Eu^{3+} (592, 619 e 700 nm). Os resultados obtidos permitiram concluir que não existe interação entre o ADN e o anião.

Neste trabalho, foram realizados dois testes em papel (em poços e μPADs) para detetar a hibridização entre a sequência de ADN do sistema de deteção e a sequência de ADN alvo, baseando-se na interação do conjugado CBM64-ZZ:anticorpo anti-biotina, imobilizado no papel, com as nanopartículas $EuW_{10}@SiO_2$-ADN. A visualização de ambos os sistemas, aquando da irradiação UV (254 nm), indica que, no estado atual, estes não são eficientes. Uma terceira abordagem, usando micropartículas de celulose (20 μm), foi então desenvolvida e, após adição de nanopartículas

$EuW_{10}@SiO_2$-ADN e deposição das micropartículas de celulose, pode observar-se fluorescência na fração depositada somente para os ensaios efetuados na presença de ADN biotinilado. Esta abordagem, em solução, baseada no uso de micropartículas de celulose confirma a viabilidade do sistema desenvolvido como marcador fluorescente para a deteção de ADN, e que poderá ser considerado uma alternativa ao uso de “quantum dots” e corantes orgânicos.

Keywords Polyoxometalates, Lanthanides, Luminescence, Biosensors, DNA, Antibodies, Cellulose

Abstract

The main goal of this thesis was the development of fluorescent paper-based sensors taking advantage of the optical properties of lanthanopolyoxometalates to obtain fast results using a portable and affordable UV lamp. The polyoxometalates (POMs) used were of the monolacunary Keggin and $[Ln(W_5O_{18})_2]^{9-}$ types containing europium cations. Core/shell-type nanoparticles (~24 nm) bearing a nucleus of the anion $[Ln(W_5O_{18})_2]^{9}$ surrounded by a silica shell were prepared and surface functionalizations were successively performed to maximize the surface's affinity for the analytes.

In the case of anion $[EuPW_{11}O_{39}(H_2O)_2]^{4-}$ ($EuPW_{11}$), a straightforward strategy was designed to investigate the potential affinity of this anion to interact with DNA relying on the use of fluorescence spectroscopy. The effect of the gradual addition of DNA to $EuPW_{11}$ aqueous solutions in the fluorescence intensity of the three main transitions of Eu^{3+} cations (592, 619 and 700 nm) was evaluated. The obtained results show that there is no interaction between the DNA and the anion.

In this work, two different paper-based tests (spots and μPADs) were developed to detect the hybridization between DNA probes and a DNA target relying on the capture by CBM64-ZZ:anti-biotin antibody conjugate immobilized on the paper and $EuW_{10}@SiO_2$-DNA. Visualization, under the excitation of a UV lamp (254 nm), of both systems indicates that in its present state the designed capture system is not efficient. A third approach relying on the use of cellulose microparticles (20 μm) was developed and, after the addition of $EuW_{10}@SiO_2$-DNA nanoparticles, the deposition of the

microparticles occurred and the assays performed in the presence of biotinylated DNA (hybridization occurred) showed increased fluorescence at the cellulose surface, contrary to the observed for the control. This approach, in solution, based on the use of cellulose microparticles emphasizes the viability of the system as a fluorescent-tag for DNA capture, that can be used as an alternative to the used quantum dots and organic dyes.

Index

List of abbreviations

Abbreviation	Designation
Ab	Antibody
AC	Acryloyl chloride
APTES	(3-aminopropyl)triethoxysilane
biot-DNA	Biotinylated DNA
DLS	Dynamic light scattering
DNA	Deoxyribonucleic acid
EDC	1-ethyl-3-(3-dimethylaminopropyl)-carbodiimide
FND	Ferrocenyl naphthalene diimide
FTIR	Fourier-transform infrared
IR	Infrared
LFA	Lateral flow assay
LFIA	Lateral flow immunoassay
LMCT	Ligand-to-metal charge transfer
Ln	Lanthanide
LnPOM	Polyoxometalates containing lanthanides
NALFA	Nucleic acid lateral flow assay
NHS	N-hydroxysuccinimide
POM	Polyoxometalates
RNA	Ribonucleic acid
SEM	Scanning electron microscopy
TCEP	Tris(2-carboxyethyl)phosphine
TEA	Triethylamine
TEOS	Tetraethyl orthosilicate
TEM	Transmission electron microscopy

THF	Tetrahydrofuran
thiol-DNA	Thiolated DNA
UV	Ultraviolet
μPAD	Microfluidic paper-based analytical device

List of Figures

List of Tables

1. Introduction

This chapter presents the two main concepts of this thesis: polyoxometalates and biosensors. Firstly, polyoxometalates are presented, as well as some of its complexes, structures and applications. Secondly, the principle behind the biosensors, their importance and their areas of action are explained.

1.1. Polyoxometalates

Polyoxometalates (POMs) are metal-oxygen clusters, mostly anionic, with an enormous range of molecular dimensions; this refers to a change from 6 up to 368 metal centres in a single molecule, see Figure 1. The building of POMs structures is based on polyhedral units with general formula MO_x (with M = Mo, W, V and sometimes Nb and x = 4, 5, 6 or 7), that assemble through oxygen bridges sharing corners, edges and faces (Figure 2) [1].

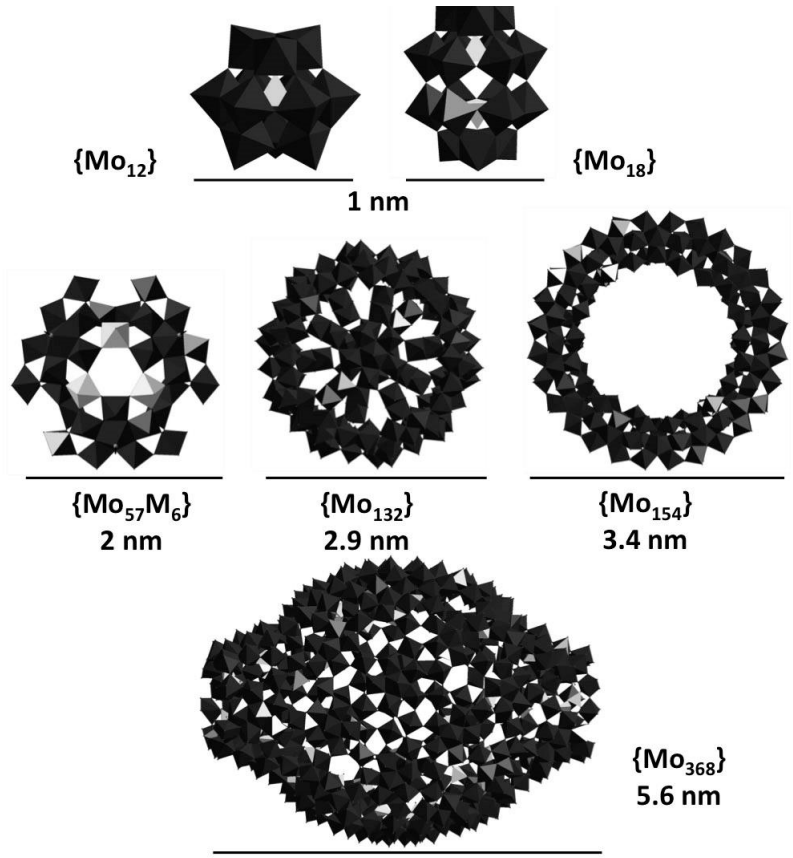

Figure 1: *Polyhedral representation of the structures of some POM clusters, all synthesized under "one-pot" reaction conditions from the Keggin {Mo_{12}} and Dawson {Mo_{18}} anions to the {$Mo_{57}M_6$}/{Mo_{132}}/{Mo_{154}} and {Mo_{368}} clusters. Colour code: MoO_6 octahedra in black; {Mo_{12}}/{Mo_{18}}: central heteroatom light grey; {$Mo_{57}M_6$}: MO_6 octahedra in grey; {Mo_{368}}: SO_4^{2-} ligands shown as light grey tetrahedra.*

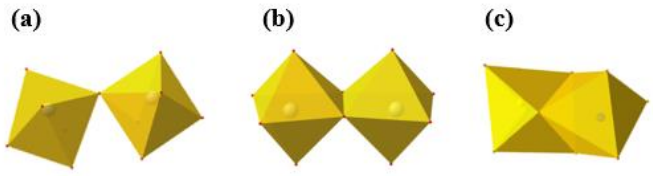

Figure 2: *Different assemblies of {MO_x} units sharing (a) corners, (b) edges and (c) faces*

There are two main classes of POMs: the isopolyanions and the heteropolyanions. Isopolyanions ($[M_xO_y]^{m-}$) are constituted by two different elements, oxygen and a metal. On the other hand, heteropolyanions of the type ($[X_zM_xO_y]^{n-}$) besides oxygen and metal atoms

are also constituted by a heteroatom (X) [2]. The M metal atoms are the ones responsible for the POM rearrangement so that they are designated as "addenda atoms" [3].

There are two classes of heteroatoms: primary and secondary. Primary heteroatoms are essential to the maintenance of the POM integrity and their removal results in the anion destruction. On the contrary, secondary heteroatoms can be removed forming different stable anionic species [4].

Due to their multifunctional properties as well as to their easy preparation methods there are many potential applications for this class of molecules. It is not only possible to perform a new type of chemistry with the clusters but also to dissolve them in organic solvents, e.g. after encapsulating them with suitable surfactant molecules, with the option of forming monolayers, thin films and hybrid materials [5,6]. Furthermore, it is possible to study their aggregation in solution leading to the formation of a new type of vesicles. [7,8].

1.1.1. Keggin anion

Keggin anion ($[XM_{12}O_{40}]^{n-}$) is one of the most representative and extensively studied heteropolyanions [9]. It is constituted by a central tetrahedron (XO_4) surrounded by twelve octahedrons (MO_6) that share edges and vertices with each other forming four groups of three octahedrons (M_3O_{13}) (Figure 3).

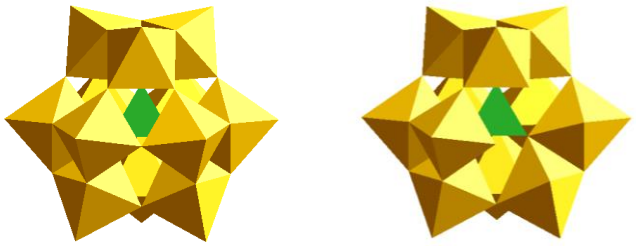

Figure 3: *Polyhedral representation of α-Keggin (left) anion and monolacunary derivative {α-XW_{11}}. Colour code: WO_6 octahedra: yellow; XO_4 tetrahedra: green*

Keggin anion can assume five different configurations, however, the α isomer is the most common one. Four rotational isomers (β, γ, δ and ε) of the Keggin anion result from a rotation of 60º of one, two, three or four M_3O_{13} groups from the α isomer (Figure 4) [10].

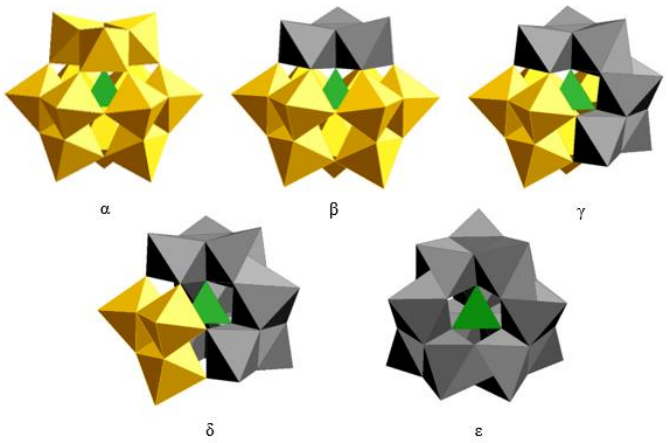

Figure 4: *Geometric isomers of the Keggin anion. Colour code: WO_6 octahedra: yellow; rotated WO_6 octahedra: grey; XO_4 tetrahedra: green*

Keggin anions can form lacunary species by removal of one or more MO^{4+} groups, using alkaline hydrolysis. Among these species, monolacunary Keggin ($[XM_{11}O_{39}]^{(p+4)-}$) emerges as the most studied one, in which its lacuna presents five potentially coordinative oxygen atoms (Figure 3 right-side).

Lacunary structures are coordinative, therefore, by reaction with metallic cations, they form monosubstituted ($[XM_{11}M'(H_2O)O_{39}]^{n-}$) and "sandwich-type" type complexes ($[M'(XW_{11}O_{39})_2]^{n-}$). Complexes from 1:1 type are mostly formed when M' is a transition metal or an element from the group *p*. In the 1:2 type complexes, M' represents a bigger cation, usually a lanthanide, which coordinates to eight oxygen ligands (four in each monolacunary fragment).

1.1.2. Wells-Dawson anion

A distinct and extensively studied heteropolyanion is the Wells-Dawson anion with general formula $[X_2M_{18}O_{62}]^{n-}$ [11], being formed by eighteen octahedrons (MO_6) (Figure 5). Wu described two isomers [12] that are now known as α and β isomers [13] In the α isomer, the two W_3O_{13} groups on the top are aligned with each other, whereas in the β isomer, one of the groups is rotated 60º. Additionally, a third isomer (γ) is possible by rotating one of the groups 120º [14]. As in the case of the Keggin anion, lacunary derivatives of the Well-Dawson anion are also known (Figure 5, right-side). The most important of these are based on the most common isomer known as α-Dawson anion.

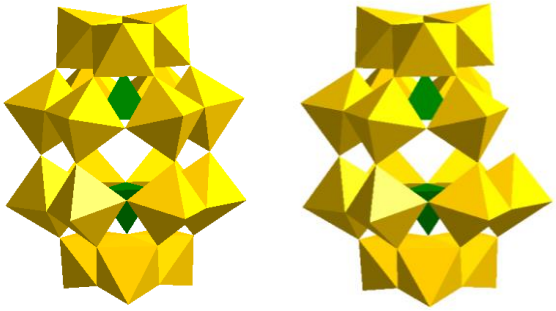

Figure 5: *Polyhedral representation of α-Dawson anion (left) and monolacunary derivative {α-X_2M_{17}} (right). Colour code: WO_6 octahedra: yellow; XO_4 tetrahedra: green*

1.1.3. Giant polyoxomolybdates

The existence of large polyoxomolybdates was unknown until 1995 when Müller *et al.* reported the synthesis and structural characterization of a very high-nuclearity cluster $[Mo_{154}O_{462}H_{14}(H_2O)_{70}]^{14-}$ ($\{Mo_{154}\}$), which has a ring topology [15,16]. The structure of the big wheel is constructed from units containing eleven Mo atoms ($\{Mo_{11}\}$), fourteen of which are linked together to form the $\{Mo_{154}\}$-type cluster that has an external diameter of 3.4 nm (Figure 6, left side). Upon slight variation of the experimental conditions, e.g by changing the pH and increasing the amount of reducing agent along with the addition of acetate ligands, the spherical shaped anion $[Mo_{132}O_{372}(CH_3COO)_{30}(H_2O)_{72}]^{42-}$ ($\{Mo_{132}\}$) can be formed [17,18] (Figure 6, right side).

Figure 6: *Comparison between the ring-shaped {Mo_{154}} (left) and spherical-shaped {Mo_{132}} (right) type clusters. Colour code: {Mo_2}: red; {Mo_1}: yellow; {Mo_{11}}: blue*

1.1.4. Polyoxometalates containing lanthanides

1.1.4.1. $[Ln(W_5O_{18})_2]^{9-}$ type polyoxometalates

$[Ln(W_5O_{18})_2]^{9-}$ type polyoxometalates (LnW_{10}) are isopolyanions constituted by two $[W_5O_{18}]^{6-}$ units coordinated by a lanthanide ion. Peacock and Weakley (1971) [19] were the first to mention the existence these complexes with Ln (III) = La, Ce, Pr, Nd, Sm, Eu, Ho, Er and Yb (Figure 7). However, it was Yamase who reported for the first time the crystal structures of these complexes, studying a wide range of lanthanide ions [20-25]. Among lanthanopolyoxometates the EuW_{10} has been the most studied and applied mainly due to its photoluminescent properties, having the highest quantum yield (67 %) reported in literature for this type of complexes [26,27].

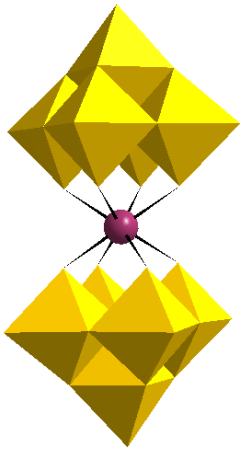

Figure 7: *Structure of a LnW_{10} type complex. Colour code: WO_6 octahedra: yellow; Lanthanide sphere: purple*

1.1.4.2. $[Ln(XM_{11}O_{39})_2]^{n-}$ type polyoxometalates

$[Ln(XM_{11}O_{39})_2]^{n-}$ type polyoxometalates are composed by two monolacunary ($[XM_{11}O_{39}]^{(p+4)-}$) type units bonded tetravalently to the lanthanide ion by four oxygen atoms from each unit (Figure 8). This complex has been applied to different areas such as catalysis [28,29], biosensors and has also been used as the building block for the fabrication of luminescent materials [30].

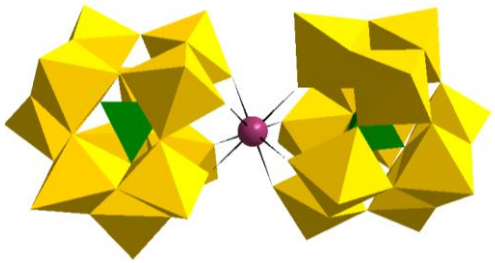

Figure 8: *Structure of* $[Eu(PW_{11}O_{39})_2]^{11-}$*. Colour code:* WO_6 *octahedra: yellow;* XO_4 *tetrahedra: green; Lanthanide sphere: purple*

1.1.4.3. $[Ln(XM_{11}O_{39})(H_2O)_y]^{n-}$ type polyoxometalates

$[Ln(XM_{11}O_{39})(H_2O)_y]^{n-}$ type polyoxometalates are constituted by a lacunary unit of the type $[XM_{11}O_{39}]^{(p+4)-}$ coordinated to a lanthanide ion by four oxygen atoms (Figure 9). In these monosubstituted structures, the coordination sphere of the lanthanide ion is usually completed by water molecules.

$[\alpha\text{-}SiW_{11}EuO_{39}(H_2O)_2]^{5-}$ has been applied to several areas due to its luminescent properties [31] and used in catalysis [32]. Luong et al. studied the hydrolytic cleavage of 4-nitrophenyl phosphate, a commonly used DNA model substrate, in the presence of this type of complexes [33].

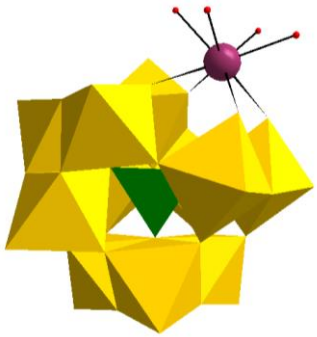

Figure 9: *Structure of* $Eu(PW_{11}O_{39})^{4-}$*. Colour code:* WO_6 *octahedra: yellow;* XO_4 *tetrahedra: green; Lanthanide sphere: purple*

1.1.4.4. $[Ln(X_2M_{17}O_{61})(H_2O)_y]^{n-}$ type polyoxometalates

$[Ln(X_2M_{17}O_{61})]^{n-}$ type polyoxometalates are composed of a lacunary $[X_2M_{17}O_{61}]^{n-}$ type unit that binds to a lanthanide ion by four oxygen atoms of the lacuna (Figure10). Due

to their luminescence, these complexes have been used as contrast agents in magnetic resonance [34] and as catalysts [35].

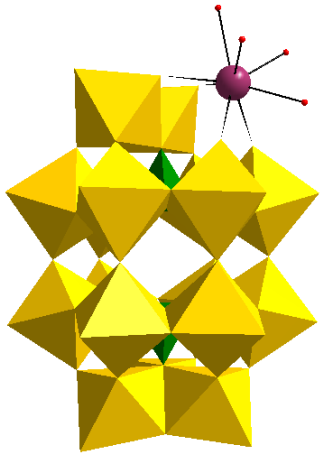

Figure 10: *Structure of a* $[Ln(X_2M_{17}O_{61})]^{n-}$ *type polyoxometalate. Colour code:* WO_6 *octahedra: yellow;* XO_4 *tetrahedra: green; Lanthanide sphere: purple*

1.1.4.5. Lanthanides ions luminescence

Luminescence is one of the most interesting properties of the lanthanide ions. Their emission covers a wide length of the electromagnetic spectrum, from the ultraviolet (Gd^{3+}) to the infrared region (Yb^{3+}, Nd^{3+} and Er^{3+}); Eu^{3+}, Tb^{3+} and Tm^{3+} emit in the visible region [36].

The highly interest on the luminescent properties of these elements lies in the fact that they have a long excited-state lifetime and in its high Stokes´ shift. However, the molar absorption coefficients (ε) of the trivalent ions are extremely low (smaller than 10 M^{-1} cm^{-1} and very often smaller than 1 or even 0.1 M^{-1} cm^{-1} [37]), meaning that only a small part of the incident radiation is absorbed by direct excitation resulting on a poor emission [38]. Yet, several strategies were developed to overcome this disadvantage such as coordination of a ligand containing an organic chromophore, usually called antennas, to the lanthanide ion. This process is designated by “antenna effect” (Figure 11) [39] and was firstly mentioned by Weissman [40]. Briefly, the energy is absorbed by the antennas, which is further transferred to the luminescent ion and then emitted. Another strategy to intensify the luminescence of the lanthanide (III) complexes is via charge-transfer states. Regarding the LnPOMs, such states are related to the interaction between the ion and the POM orbitals. In these complexes,

occur ligand-to-metal charge transfer phenomena (LMCT) associated with the O → Ln and O → M transitions [41,42].

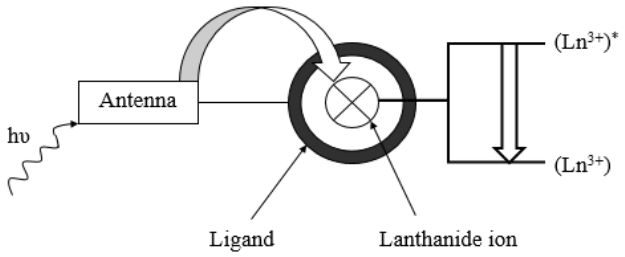

Figure 11: *Principle of the antenna effect. The energy transfer is favoured by the short distance between the antenna ligand and the lanthanide ion*

1.1.2. Encapsulation of POM clusters and functionalization of silica nanoparticles

Lanthanopolyoxometalates are of both fundamental and technological interest due to their characteristic luminescent properties, such as extremely sharp emission bands, high Stokes´ shift long lifetime and high quantum yield. Over the last decade the development of core-shell nanoparticles has been extensively reported, considering their potential applications, which include new clinical diagnosis platforms [43]. Coating nanoparticles with a silica shell, using microemulsion methods, has become a widely used technique [44]. The high stability in water, optical transparency, large surface area along with the relatively ease of surface functionalization makes silica a suitable candidate from the encapsulation of POMs. Thus, opening new possibilities to explore the luminescent properties of these species in a wide variety of applications, ranging from catalysis to biosensing. [45,46].

Silica surface functionalization with primary amine groups may follow two methods: the co-condensation method and the post-synthesis grafting method. The first method consists on the use of silica precursors, such as tetraethyl orthosilicate (TEOS) (Figure 12), and an organosilane, such as (3-aminopropyl)triethoxysilane (APTES) during a sol-gel process [47]. In the second procedure, the silica is previously synthesized and then functionalized with an organosilane.

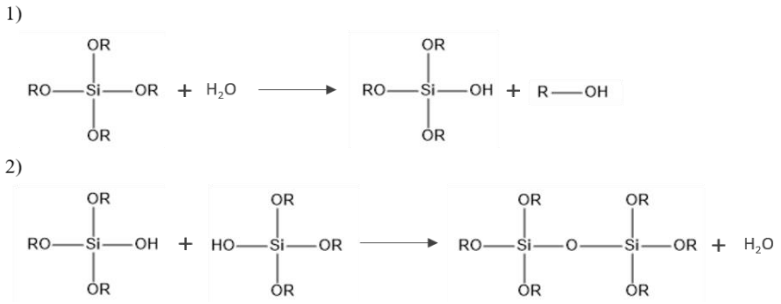

Figure 12: *TEOS hydrolysis (1) and condensation (2) mechanisms*

1.1.3. POMs and POM-complexes in bioapplications

Over the last years, the research group of Prof. Tatjana N. Parac-Vogt has been exploring the reactivity of different classes of POMs as catalysts for the hydrolysis of biologically important molecules and their model systems, such as POM catalyzed peptide bond hydrolysis in peptides and proteins [48,49]. Although POMs are traditionally employed in catalysis, they have also been shown to exhibit potent antiviral [50], antibacterial [51], antitumor [52] and redox [53] activity, initiating substantial interest in the potential medical applications of POMs. Yet, despite their proven potential in bioapplications, the use of POMs in biosensors development is still lacking.

1.2. Biosensors

In a world running towards the "personalized medicine", deep understanding of biological processes and extreme quality control of food and medicine is essential. Regarding this, biosensors are gaining increasingly relevance in modern and future society. Generally, a biosensor is a small device with recognition properties for a selective bio-analysis [54-56] that enables the detection of the presence and/or absence of an analyte. Nowadays, the most common biosensors are based in immunoassays or in molecular recognition, where the coupling of a biological recognition element with a physical transducer to convert the biological interaction or phenomenon into a signal which can be proportional to the concentration of analytes, making it quantitative, or in some causes just indication of presence or absence of an analyte - qualitative [57-62]. A basic biosensor assembly includes a receptor, a transducer and a processor (Figure 13). The recognition

elements may be cells, antibodies, enzymes, nucleic acids, metabolites or hormones, forming a recognition layer that is integrated with the transducer by adsorption, cross-linking or covalent binding.

Overall, the performance of a biosensor depends of three parameters: its ability to immobilize recognition elements maintaining their intrinsic properties, the accessibility of the recognition element to the relevant analyte in the sample, and low non-specific recognition both to other species present in sample or to the materials in the device, which can increase noise in the measurement, increase "false positive" results and overestimate the presence of the analyte.

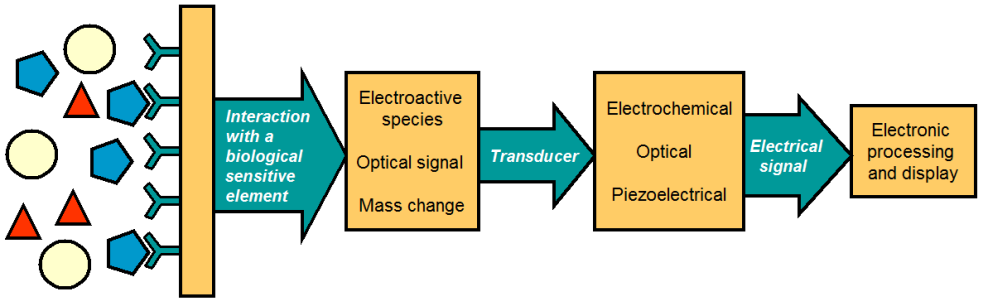

Figure 13: *Scheme of the basic components of a biosensor* [54]

1.2.1. Nucleic acid biosensor

Genetic testing to access the presence of nucleic acids within a sample have been widely used in biosensors and bio-analytical assays, due to their wide range of physical, chemical and biological activities [63]. In nucleic acid-based biosensors, sensing elements are either oligonucleotides, with a known sequence of bases, or a fragment of DNA or RNA. These biosensors are based on the highly specific hybridization of complementary strands of DNA/RNA molecules or play the role of a highly specific receptor of biochemical or chemical species [64-66]. The development of molecular-based diagnostics analyses of genomic sequences have offered a highly sensitive and quantitative method for the detection of infectious diseases, pathogens and genetic variations. Additionally, nucleic acid recognition is also being explored in the development of imaging tools, mostly associated with nanotechnology, that have been medically applied as non-invasive methods of diagnosis [67-69].

1.2.2. Immunosensors

Antibodies (Ab) are proteins produced by the immune system in response to the presence of a foreign substance, also known as antigen. These molecules function is the recognition and binding to a specific antigen and to mediate its removal from the body. They are 'Y'-shaped immunoglobin (Ig) that is constituted by four polypeptide chains: two heavy (H) – linked to each other by disulphide bonds - and two light (L) (Figure 14). Each of the chain has a constant (C) and a variable part (V) being the variable part responsible for the specificity and binding to the antigen [70].

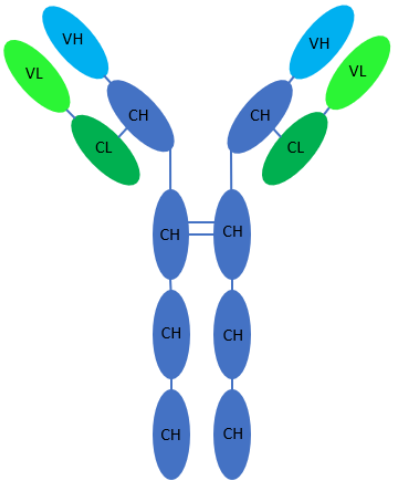

Figure 14: *Structure of an antibody*

Immunosensors represent a family of biosensors that contain an immobilized molecular recognition molecule that will have an antibody-antigen response towards a biological component (antibody, antigen) being an immunological receptor for recognition of molecules. They can either be designed for the detection of antibodies or antigens. Usually, the detection of antibodies is preferred because the use of antibodies as recognition elements may lead to a loss of their affinity during the immobilization process, which affects the detection limit, sensitivity and overall performance of the immunosensor [71]. Although preferable, this approach limits the application of these sensors, because most of the interest analytes are non-antibodies molecules. For this reason, diverse approaches have been developed, including functionalizing of the surface with specific reactive groups and using different chemistry procedures (such as carbodiimide, succinimide ester, maleinimide or periodate) or engineering it with nanostructures, to increase the efficiency of the Ab

immobilization with specific orientation without affecting its overall “performance” [72]. Covalent immobilization is the most studied immobilization strategy, as it involves surface modification in order to obtain reactive groups (such as thiol, carboxyl or amine groups) on the surface for the subsequent Ab immobilization and facilitates the long-term storage, reusability of immunosensors and increase reproducibility.

Immobilizing Abs onto the sensor surface by targeting amine groups present in the Ab, usually by reaction with carboxylic groups through carbodiimide protocols, is a widely used form of covalent immobilization, due to the relatively easy access to these groups and controlled chemistry. However, a disadvantage of this strategy is that Abs can have several amine groups in its constitution, leading to an immobilization of the Ab in a less favoured form. In the example of coupling of the amine groups of Abs with terminal carboxylated gold, the amine groups on Abs bind with succinimide esters (formed by the reaction between carboxylic acid, 1-ethyl-3-(3-dimethylaminopropyl)-carbodiimide (EDC) and n-hydroxysuccinimide (NHS)) to form a covalent linkage [73]. Thiol groups can also be used for Ab immobilization, usually they provide a more homogeneous immobilization in comparison with amine coupling. Coupling Abs with a sensor surface using a thiol group is typically based on thiol–disulphide exchange between thiol groups on the Ab and active disulphides added to the surface. Ab fragments orientally immobilized have been shown to achieve an enhanced antigen-binding ability, compared with the randomly immobilized Abs, using amine groups [74].

1.2.3. Lateral flow assay as detection strategy

Based on the recognition elements used, lateral flow assays (LFAs) can be divided in two classes: the lateral flow immunoassay (LFIA, in which antibodies are exclusively used as recognition elements) and the nucleic acid lateral flow assay (NALFA). LFA is a paper-based platform for the detection and quantification of analytes in complex mixtures. Low production costs and easy fabrication of LFAs resulted in the expansion of its applications to multiple areas. LFA-based tests are widely used for the qualitative and quantitative detection of specific antigens [75] and antibodies [76], as well as products of gene amplification [77,78].

A liquid sample containing an analyte of interest moves through the matrix, due to capillary action, on which molecules that can interact with the analyte are attached. As shown in Figure 15, the sample is applied in one extremity of the device, which is impregnated with a buffer containing salts and surfactants that minimizes interaction between the sample and surface of the device and favours interaction of the sample with the detection system. Labelled molecules, that will function as signal source, together with the sample will flow through the device towards test and control zones. As the sample flows along the membrane these labelled molecules can interact with the analyte present in the sample and further attach the molecular recognition molecules present in the test zone [79].

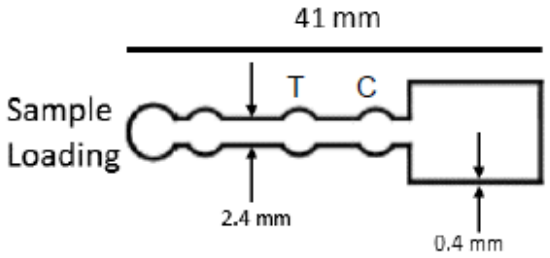

Figure 15: *Design of a microfluidic paper-based analytical device (μPAD). The regions T and C correspond to the Test and Control spots, respectively* [80]

1.2.3.1. Labels used in LFAs

High sensitivity and selectivity are two of the most important parameters when it comes to select a label for the LFA development. Due to their signal amplification, easy production and functionalization, nanomaterials have been attracting great interest within this field [81]. Nanoparticles because of their ability to produce optical signal, including fluorescence, colour changes by assemblies and aggregations and simply colour accumulation in the test zone [82], have emerged as the preferable labels in LFA technology, such as gold nanoparticles [83], carbon nanoparticles [84] quantum dots [85] and doped silica nanoparticles [86]. Enzymes can also be used as labels in LFAs based on the enzyme-substrate reactions for colour formation that can be visible to the naked eye [87].

Gold nanoparticles

Colloidal gold nanoparticles are the most commonly used labels in LFA. Colloidal gold is inert and allows the synthesis of almost perfect spherical particles that can be easily

functionalised. Their unique features include environment friendly preparation, high affinity for biomolecules, enhanced stability, exceptionally higher values for charge transfer and good optical signalling [88]. Optical signal of gold nanoparticles in colorimetric LFA can be amplified by deposition of silver, gold nanoparticles and enzymes [89,90].

Carbon nanoparticles

Due to their black colour, carbon nanoparticles can be easily detected with high sensitivity. On one hand, colloidal carbon can be functionalised with a large variety of biomolecules for detection of low and high molecular weight analytes which is a great advantage. On the other hand, the presence of irregular shaped particles and nonspecific adsorption of proteins and biomolecules are major problems with colloidal carbon. [91].

Quantum dots

The conventional systems based on colorimetric labels as reporters have limitation in detecting the target analyte at low concentration. Hence, systems using different labels have been developed to answer this need. Fluorescent molecules have been widely used in LFA as labels to solve this limitation once the fluorescence intensity is proportional to the concentration of analyte in the sample. Quantum dots are among these molecules and display unique electrical and optical properties. These semiconducting particles present a high Stokes´ shift, being easy to separate the excitation from the emission, even with the naked eye. Additionally, they are water soluble and can be easily combined with biomolecules and have emerged as a substitute to organic fluorescent dyes. Quantum dots can retain their fluorescent properties within cells and organisms because of their inorganic nature (limited or absence of photobleaching) [92]. However, the formation of quantum dot-biomolecule complexes is difficult which constitutes an inconvenient regarding their bioapplications compared to other nanoparticles [93]. Moreover, these materials typically present high toxicity [94].

Silica nanoparticles

Recently, fluorescence-doped silica nanoparticles have shown advantages over other fluorophores as highly sensitive and photostable fluorescence probes for bioapplications [95]. During the synthesis, the fluorescence molecules are trapped inside silica matrix protecting them from the outer environment resulting in dye photostability and probe sensitivity improvement. Using conventional silica-based chemistry, specific functional

groups could be easily added on particle surface to provide reactive sites for covalent bioconjugation [96,97]. Based on their unique optical properties, as well as versatility in synthesis and surface modification, fluorescence-doped silica nanoparticles are a good alternative as fluorescence probes for a LFA.

2. Objectives of the work

Different classes of lanthanopolyoxometalates will be explored as building blocks for the fabrication of biosensors. The aims of the work to be developed in the course of this thesis are as follows:

- Synthesize and characterize different polyoxometalates containing lanthanides
- Coat the prepared POMs with a protective silica shell providing a suitable surface for posterior functionalization and DNA immobilization via “click” chemistry
- Fabricate biosensors using the POMs-based materials as fluorescent-tag

3. Synthesis and characterization

This chapter describes the selected procedures for the synthesis of the lanthanopolyoxometalates and lanthanopolyoxometalate nanoparticles prepared, as well as all the characterization techniques used in their analysis. The procedures/strategies used for the functionalization, DNA immobilization at the nanoparticles' surface and for the development of cellulose biosensors are also presented.

3.1. Synthesis of lanthanopolyoxometalates

3.1.1. Synthesis of $K_7[PW_{11}O_{39}].nH_2O$ [98]

Dodecatungstophosphoric acid (20 g) was dissolved in 100 mL of hot water (40 ºC). 1 g of sodium chloride (NaCl) was added to the previous solution. An aqueous solution of 1 M of potassium hydrogencarbonate was added dropwise under vigorous stirring until pH of the solution became 5. After 10 minutes, the reaction mixture was filtered, and the filtrate was concentrated and allowed to stand at room temperature for 48 h. After, 8 g of potassium chloride (KCl) was added and the solution stored in the fridge to precipitate. The white crystalline salt that obtained was filtered and recrystallized in hot water.

3.1.2. Synthesis of $K_4[EuPW_{11}(H_2O)_2O_{39}].nH_2O$ [99]

$PW_{11}O_{39}^{7-}$ (6.09 g) was dissolved in 25 mL of water at 40 °C and the solution was added dropwise to 10 mL of a europium nitrate hexahydrate ($Eu(NO_3)_3{\cdot}6H_2O$) aqueous solution (0.2 M). The resulting solution was stirred vigorously for 3 minutes followed by the addition of NaCl (0.87 g) and 105 mL of ethanol. The white precipitate was collected by filtration and dried under suction.

3.1.3. Synthesis of $Na_9[Eu(W_5O_{18})_2].nH_2O$ [17]

Sodium tungstate dihydrate ($Na_2WO_4{\cdot}2H_2O$) (5.01 g)was dissolved in 7 mL of water and the pH adjusted to 7 with glacial acetic acid (CH_3CO_2H). The solution was heated to 90 ºC and a hot solution containing 0.65 g of $Eu(NO_3)_3{\cdot}6H_2O$ in 2 mL of water was added dropwise followed by the addition of 8 mL of a hot aqueous solution with 1.02 g NaCl. The solution was stirred for 30 minutes at 90 ºC and then cooled to room temperature before storing in the fridge. After a few days (3-4 days), the precipitate was collected by filtration and washed with cold water.

3.1.4. Fourier-transform infrared and Raman spectroscopy

Vibrational spectroscopy (FTIR and Raman) is a fundamental tool for polyoxometalate characterization, providing useful information about the structure of different anions. Figure 16 shows the FTIR (Tensor 27, Bruker Co.) spectra (potassium bromide pellet) of anions EuW_{10}, PW_{11} and $EuPW_{11}$.

One of the characteristic vibration bands of EuW_{10} around 945 cm^{-1} corresponds to the vibrations of W=O bonds [100]. It is also possible to observe the similarities between the PW_{11} and the $EuPW_{11}$ profiles what was expected due to their similar chemical structure. While the vibrations of the W-O-W bonds bands appear on a wider range (785–923 cm^{-1}). The band at 1080 cm^{-1} corresponds to the P-O stretching modes of the central PO_4 tetrahedron [101].

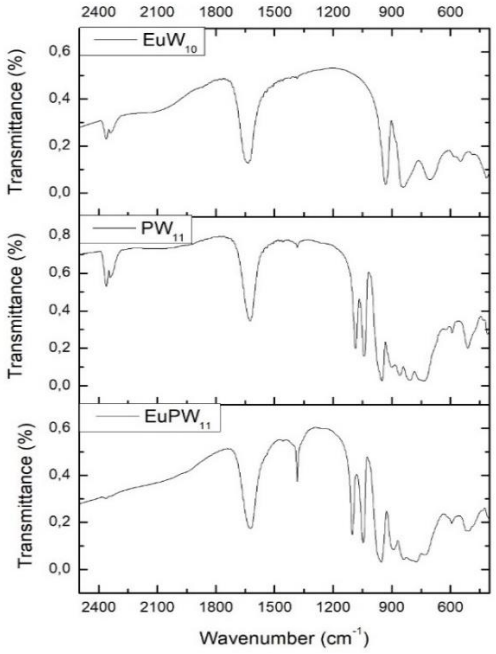

Figure 16: *FTIR spectra of anions EuW_{10}, PW_{11} and $EuPW_{11}$*

Figure 17 shows the Raman (RFS 100/S, Bruker Co., Nd:YAG laser, 1064 nm excitation) spectra of the anions EuW_{10} and $EuPW_{11}$. The characteristic bands of the POM, namely the terminal W=O and W-O-W bridging vibrational modes, are observed around 945 cm^{-1} and between 785–923 cm^{-1}, respectively. It is also possible to observe the band corresponding to the P-O stretching mode of the central PO_4 tetrahedron around 1000 cm^{-1}.

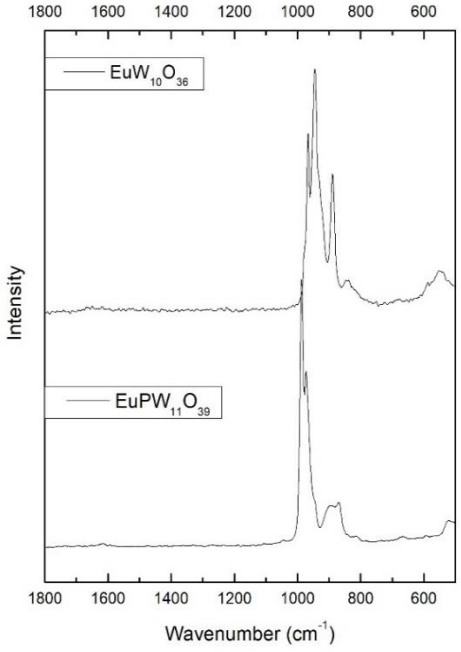

Figure 17: *Raman spectra of anions EuW_{10} and $EuPW_{11}$*

3.1.5. Fluorescence spectroscopy

To characterize the fluorescence profile of the materials synthesized, absorption and emission analysis were performed (Spectrofluorometer FP-8300, JASCO) in the wavelength range of 300-750 nm. Figure 18 shows the excitation and emission spectra of anions EuW_{10} and $EuPW_{11}$ (solid state). The excitation spectrum of EuW_{10} is composed of narrow and sharp peaks that correspond to the intra-$4f_6$, $^7F_0 \rightarrow {}^5D_{4\text{-}1}$, $^5G_{2\text{-}5,}$ $^5L_6$ and $^7F_1 \rightarrow {}^5D_{2,1}$ transitions. The emission spectrum shows the characteristic peaks of Eu^{3+} attributed to the $^5D_0 \rightarrow {}^7F_{0\text{-}4}$ transitions (578, 592, 619, 650 and 700 nm) corresponding to the characteristic red/orange emission (Figure 19). In the case of anion $EuPW_{11}$ the excitation spectrum shows several peaks corresponding to the intra-$4f_6$. Once again, the emission spectrum shows the characteristic red/orange emission corresponding to transitions between the first excited state $^5D_0$ and the $^7F_{0\text{-}4}$ levels.

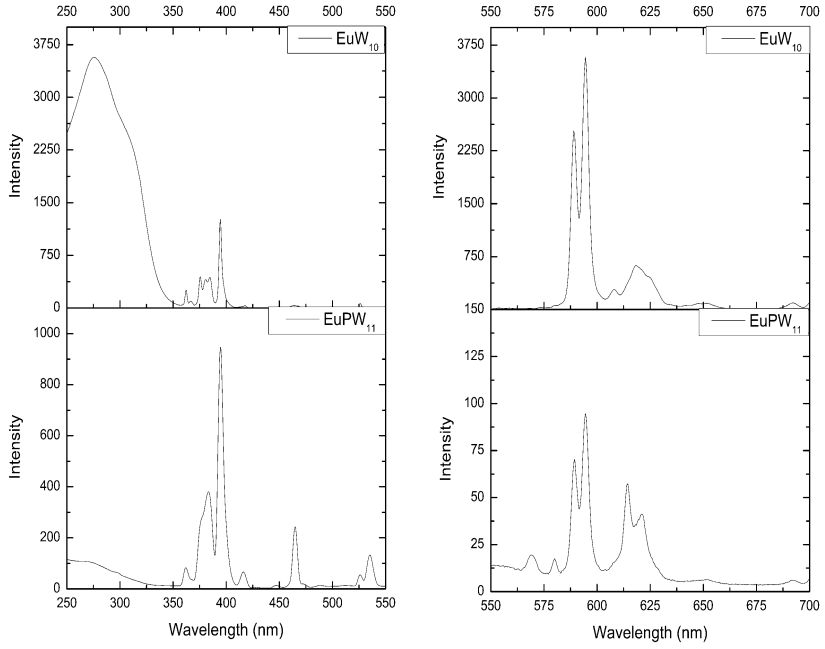

Figure 18: *Left: excitation spectra (fixing the emission at 595 nm); right: emission spectra of the anions EuW_{10} (excited at 276 nm) and $EuPW_{11}$ (excited at 395 nm)*

The profiles obtained for the EuW_{10} were expected as the compound has its maximum excitation peak around 280 nm (corresponding to UV radiation) and its maximum emission peak around 600 nm (corresponding to orange radiation which is characteristic of europium complexes). However, it is interesting that the $EuPW_{11}$ maximum excitation peak

was located at around 395 nm. This difference may be due to the dissimilar environments of the Eu^{3+} in both POMs, arising from the fact that its coordination sphere is completed by water molecules.

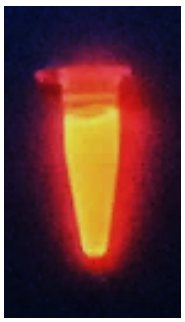

Figure 19: *Aqueous solution of EuW_{10} while being excited with UV radiation (254 nm)*

3.2. Synthesis of core-shell lanthanopolyoxometalate-silica nanoparticles

In this section is described the synthesis and characterization of core-shell nanoparticles of the type POM@SiO_2 consisting of a POM core encapsulated in an amorphous silica layer. These nanoparticles were prepared by a reported method based on the alkaline hydrolysis of tetraethoxysilane in the presence of POMs using a reverse microemulsion method. The anion $[Eu(W_5O_{18})_2]^{9-}$ (EuW_{10}) was selected for the encapsulation due to its promising luminescent properties.

3.2.1. Synthesis of $[Eu(W_5O_{18})_2]$@SiO_2

Two microemulsions were prepared, one containing 2.22 mL of Triton X-100, 2.31 mL of 1-octanol, 9.31 mL of cyclohexane, 200 μL of tetraethyl orthosilicate (TEOS) and 1.00 mL of a EuW_{10} aqueous solution (50 mg/mL) (A); and the other containing 2.22 mL of Triton X-100, 2.31 mL of 1-octanol, 9.31 mL of cyclohexane and 200 μL of ammonium solution (B). After stirring for 20 minutes at room temperature, the microemulsion B is added to the microemulsion A and the mixture is stirred for 24 h at room temperature. After 24 h, 150 mL of acetone were added to the mixture that is kept undisturbed for 3 days in order to promote the precipitation of the nanoparticles. Then, the mixture is centrifuged (3220 g, 15 minutes), and the nanoparticles washed with water and anhydrous ethanol.

3.2.2. Functionalization of the $[Eu(W_5O_{18})_2]@SiO_2$ with (3-aminopropyl)triethoxysilane

In our design, a critical step is the functionalization with a primary amine, from 3-aminopropyltriethoxysilane (APTES), which will allow further functionalization and DNA immobilization, and to do so, two different approaches were used to prepare $EuW_{10}@SiO_2$ particles. The first strategy was an adaptation of a reported method by Yuan *et al.* (2004) [44] and it consists in the preparation of an ethanolic solution of the $EuW_{10}@SiO_2$ nanoparticles (0.5 mg/mL) and the posterior addition of 150 µL of APTES. After stirring for 24 h, the mixture is centrifuged (3220 g, 15 minutes), and the nanoparticles washed with water and anhydrous ethanol (Figure 20).

The second method, denominated "*in-situ*", consists in the preparation of two microemulsions, one containing 2.22 mL of Triton X-100, 2.31 mL of 1-octanol, 9.31 mL of cyclohexane, 150 µL of TEOS, 50 µL of APTES and 1.00 mL of a EuW_{10} aqueous solution (50 mg/mL) (A); and the other containing 2.22 mL of Triton X-100, 2.31 mL of 1-octanol, 9.31 of mL cyclohexane and 200 µL of ammonium solution (B). After stirring for 20 minutes at room temperature, the microemulsion B is added to the microemulsion A and the mixture is stirred for 24 h at room temperature. After 24 h, 150 mL of acetone were added to the mixture that is kept undisturbed for 3 days in order to promote the precipitation of the nanoparticles. Then, the mixture is centrifuged (3220 g, 15 minutes), and the nanoparticles washed with water and anhydrous ethanol. In this case, the simultaneous hydrolysis and co-condensation of TEOS and APTES, resulted in a silica coating of the EuW_{10} and a successful incorporation of functional amino groups on the surface of the particles.

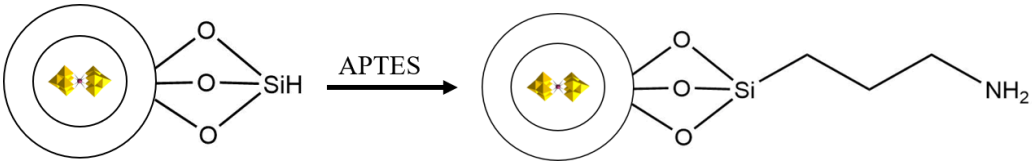

Figure 20: *Schematic representation of APTES functionalization of $EuW_{10}@SiO_2$ nanoparticles*

3.2.3. Infrared spectroscopy

As it is shown in Figure 21, after the encapsulation and the APTES functionalization, EuW_{10} maintained its chemical structure. The large band observed at 1050 cm^{-1} corresponds to the asymmetric stretching mode of the Si-O-Si bonds. The successful APTES functionalization (primary amine group, $R\text{-}NH_2$) was confirmed by the appearance of new bands between 1300 and 1700 cm^{-1} corresponding to: the deformation δ(N-H) of amine groups (around 1560 cm^{-1}), to the deformation and torsional vibrations of C-H bonds of the alkyl chain (around 1475 and 1384 cm^{-1}, respectively) and to the stretching mode ν(C-O) (around 1305 cm^{-1}) of the ethoxy groups.

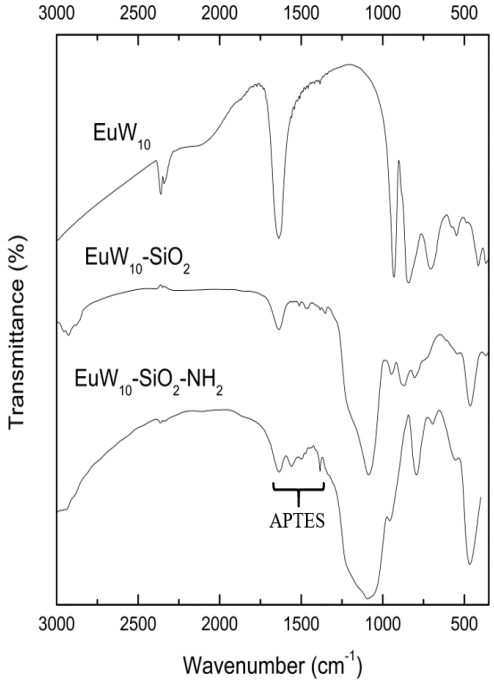

Figure 21: *FTIR spectra of EuW_{10}, $EuW_{10}@SiO_2$ and $EuW_{10}@SiO_2\text{-}NH_2$*

3.2.4. Fluorescence spectroscopy

Figure 22 shows the excitation and emission spectra of $EuW_{10}@SiO_2\text{-}NH_2$. The excitation spectrum exhibits a large band and a couple of low intensity bands corresponding to intra-4f transitions. The emission spectrum shows the characteristic peaks of Eu^{3+} attributed to the $^5D_0 \rightarrow {}^7F_{0\text{-}4}$ transitions corresponding to the characteristic red/orange emission. Therefore, it is possible to observe that the photophysical properties of the EuW_{10} are maintained after encapsulation and functionalization.

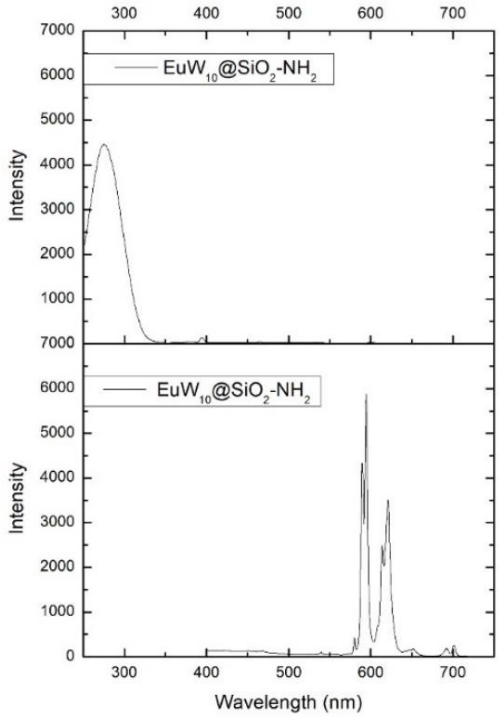

Figure 22: *Excitation (fixing the emission at 595 nm) and emission (fixing the excitation at 276 nm) spectra of* $EuW_{10}@SiO_2\text{-}NH_2$

3.2.5. Dynamic light scattering and Zeta potential

Dynamic light scattering (DLS) was used to estimate the size distribution of the prepared nanoparticles and zeta potential measurements were performed to estimate the determining the surface charge. These analyses were performed using the Zetasizer Nano ZS (Malvern Instruments).

The hydrodynamic diameter found for $EuW_{10}@SiO_2$ was 90 nm and for $EuW_{10}@SiO_2\text{-}NH_2$ was 361 nm. Although the thickening of the silica shell was expected, due to the APTES condensation, the observed increase of the hydrodynamic diameter can also be attributed to the polydispersity of the nanoparticles, since APTES can interfere in micelles formation. The average surface charge was evaluated, at a constant pH of 7.2, and the results confirm that the APTES functionalization was successfully done, since an increase of the charge from -12.7 mV ($EuW_{10}@SiO_2$) to -4.52 mV ($EuW_{10}@SiO_2\text{-}NH_2$) was observed.

3.2.6. Transmission electron microscopy and Scanning electron microscopy

Transmission electron microscopy (TEM – H9000, Hitachi) and scanning electron microscopy (SEM - SU-70, Hitachi) were used to evaluate the morphology, size and shape of the nanoparticles. The transmission electron microscopy (TEM) images of the $EuW_{10}@SiO_2$ nanoparticles (Figure 23) show morphological uniform nanosized spheres, composed of a core of EuW_{10} (darker centre) which is coated with amorphous SiO_2. The estimated diameter of the nanospheres is 23.8 ± 1.2 nm containing a POM core that is 6.3 ± 0.5 nm wide. Due to an equipment malfunction were unable to characterize the $EuW_{10}@SiO_2$-NH_2 nanoparticles.

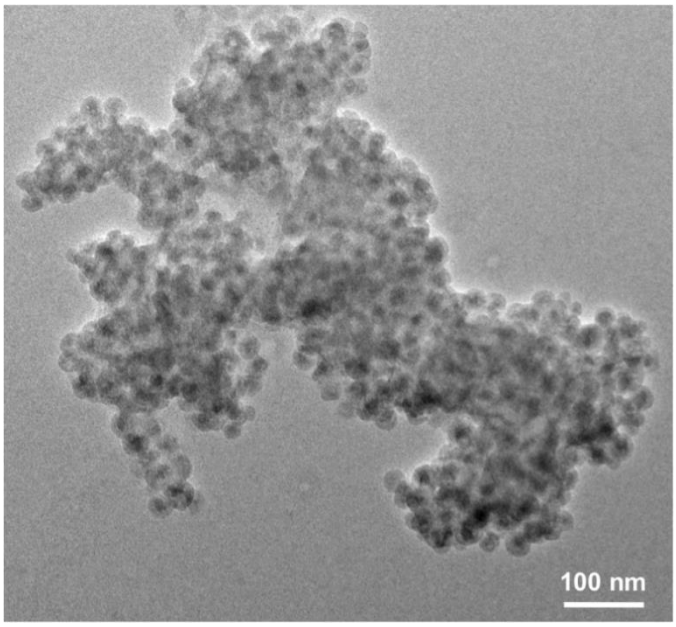

Figure 23: *TEM images of $EuW_{10}@SiO_2$ nanoparticles*

Scanning electron microscopy (SEM) was used to investigate the morphology of the prepared nanoparticles. Figure 24 shows the SEM images of $EuW_{10}@SiO_2$ nanoparticles exhibiting a spheroid morphology with an average diameter of 72.0 ± 6.5 nm. The SEM images (Figure 25) of the $EuW_{10}@SiO_2$-NH_2 nanoparticles show a certain degree of agglomeration and the spheroid shape is maintained, comparing with the non-functionalized particles, with an average diameter of 83.9 ± 6.1 nm. This increase is not surprising since the hydrolysis and condensation of APTES results in an increase of the silica shell.

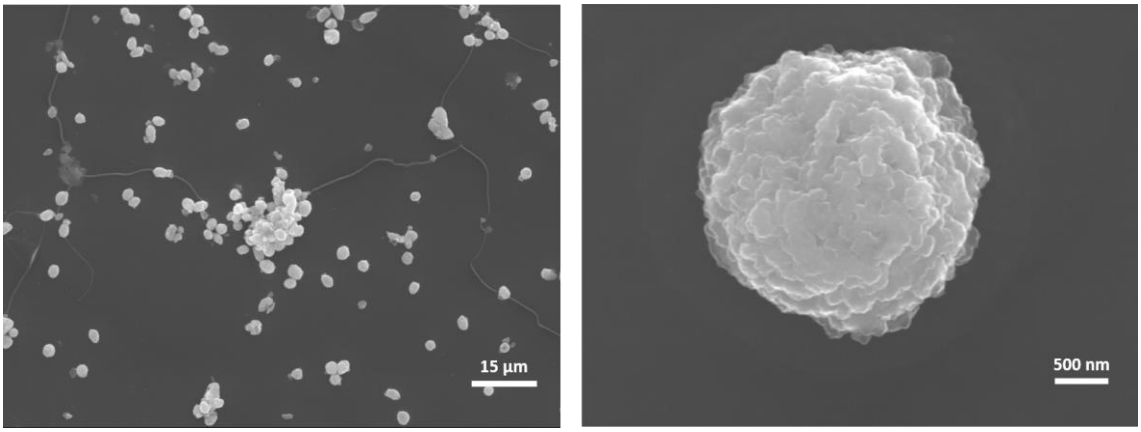

***Figure 24**: SEM images of $EuW_{10}@SiO_2$ nanoparticles*

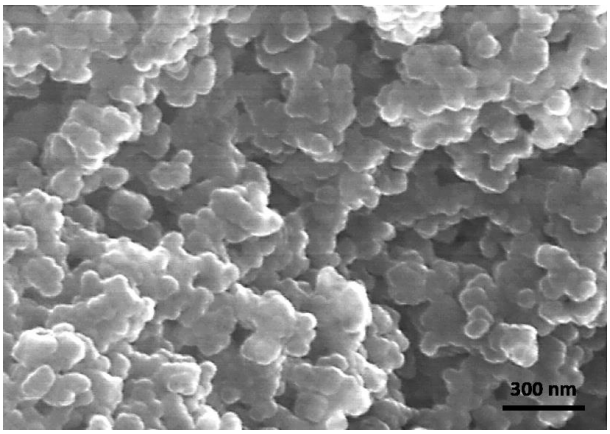

***Figure 25:** SEM image of $EuW_{10}@SiO_2$-NH_2 nanoparticles*

As expected, the energy-dispersive X-ray spectroscopy (EDS – QUANTAX 400, Bruker Co.) analysis revealed that the nanoparticles shown in the figure above contain europium, tungsten and silicium in their constitution (Figure 26).

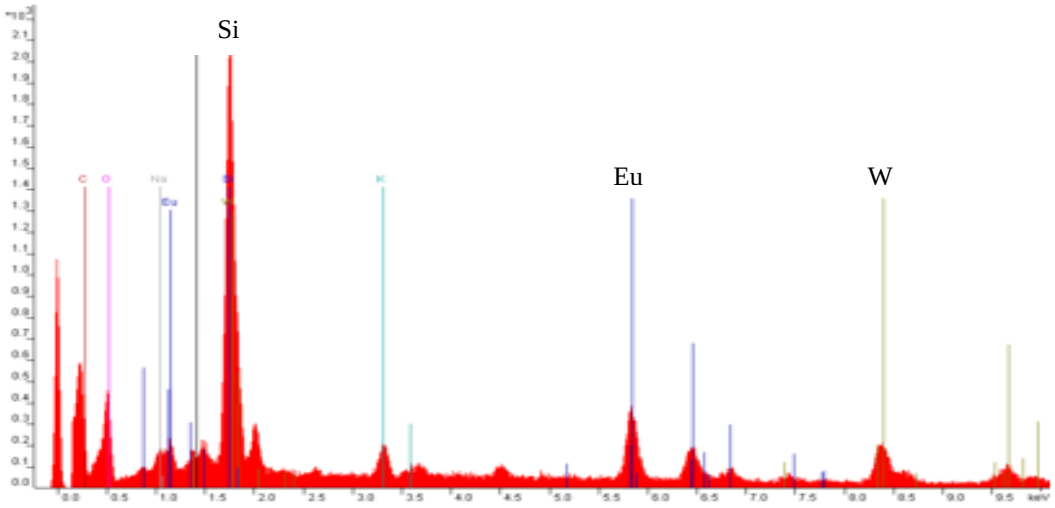

***Figure 26:** EDS spectrum of $EuW_{10}@SiO_2$-NH_2*

3.2.7. Functionalization of the $[Eu(W_5O_{18})_2]$@SiO_2-NH_2 with acryloyl chloride [102]

After the characterization, the EuW_{10}@SiO_2-NH_2 nanoparticles were further functionalized with acryloyl chloride. During this functionalization the primary amines (present in the nanoparticles) will react with the chloride present in the acryloyl molecule, conferring an -ene group that will allow the immobilization of a DNA contain a thiol group, using a thiol-ene click chemistry reaction (Figure 27).

2.35 g of EuW_{10}@SiO_2-NH_2 and 1.46 mL of triethylamine (TEA) were dissolved in 20 mL of anhydrous methanol and the solution was stirred for 30 minutes in an ice bath. Then, 1.22 mL of acryloyl chloride (AC) in 1.00 mL of tetrahydrofuran (THF) and 2.20 mL of TEA in 2.00 mL of anhydrous methanol were added dropwise. The ice bath was removed, and the mixture is stirred for 2 h at room temperature. After that time, the mixture was centrifuged (3220 g, 5 minutes), and the nanoparticles washed three times with water.

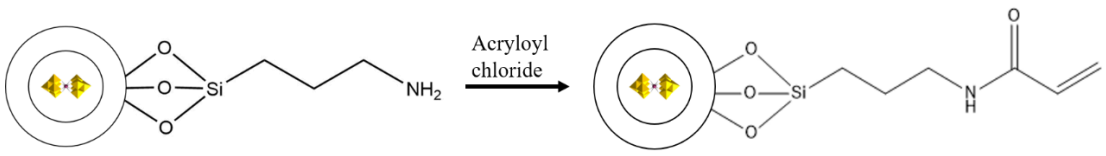

Figure 27: *Schematic representation of AC functionalization of EuW_{10}@SiO_2-NH_2 nanoparticles*

3.2.8. Functionalization of the $[Eu(W_5O_{18})_2]$@SiO_2-AC and the $Eu(PW_{11}O_{39})$ with thiol-DNA

The thiol-DNA probe used in this project was purchased from STAB-Vida and has the following sequence:

sh_5´-ttg aag cct gtt ctc gga gag-3´

The functionalization of the nanoparticles was performed as follows. To 0.50 mL of nanoparticles aqueous solution (1.62 mg/mL), 100 µL of a thiol-DNA aqueous solution was added and the solution was incubated for 2 h. Prior to addition, the thiol-DNA solution was treated with a tris(2-carboxyethyl)phosphine solution (TCEP) (Figure 28), to guarantee a full reduction of the DNA probe (reduction of the S-S bonds to -SH), it. After the incubation, the nanoparticles were washed 3 times with water.

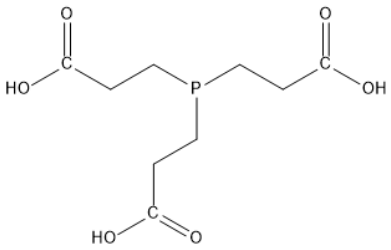

Figure 28: *Chemical structure of TCEP*

The covalent immobilization of the DNA to the nanoparticles was performed via thiol-ene "click" chemistry reaction which is simply a hydrothiolation of a C=C bond. Figure 29 illustrates the DNA functionalization of the nanoparticles.

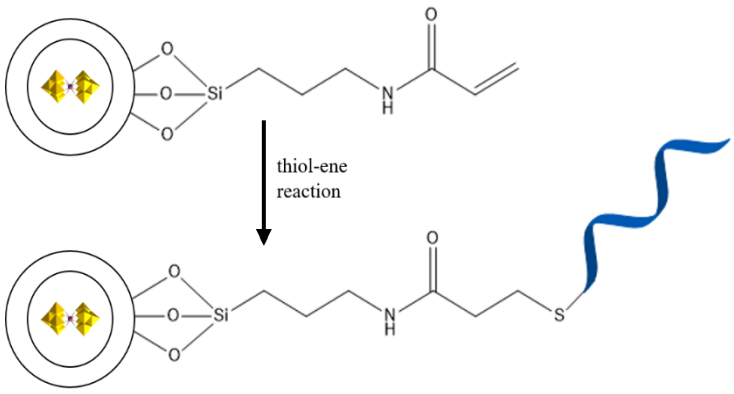

Figure 29: *Schematic representation of DNA functionalization of $EuW_{10}@SiO_2$-AC nanoparticles via thiol-ene reaction*

Despite knowing that the $EuPW_{11}$ anion was not ideal for the development of cellulose-based biosensors, because the UV lamp available (254 nm) was not the proper to efficiently excite this anion, we tried to take advantage of the uncompleted europium coordination sphere to directly interact with the DNA probe. The interaction between the lanthanide and the DNA would be made through coordination to phosphate groups (PO_4^{3-}). However, as it is shown in Figure 30, no notable differences were obtained in the fluorescence profile after the addition of different concentrations of the DNA aqueous solution. One possible reason for this apparent lack of interaction may be the low accessibility to the phosphate groups, contrary to the observed for 4-nitrophenyl phosphate, commonly used as DNA model [34].

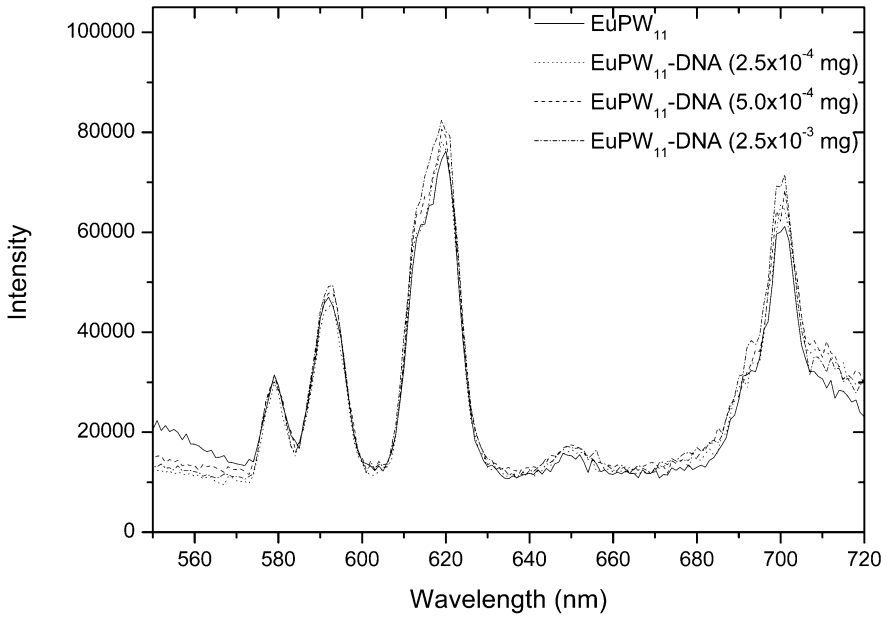

Figure 30: *Emission spectra of $EuPW_{11}$ and $EuPW_{11}$ functionalized with different quantities of DNA - $2.5x10^{-4}$ mg, $5.0x10^{-4}$ mg and $2.5x10^{-3}$ mg (excited at 395 nm)*

3.2.9. Zeta potential

Zeta potential is a technique that allows the determination of surface charge of nanoparticles. After functionalization with acryloyl chloride, containing an -ene group, the zeta potential of the particles decreased from -4.52 mV for the NH_2-coated nanoparticles to -21.33 mV for the acryloyl-functionalized particles. One possible explanation for this is the fact that these measurements give a mean value for the particle charge. In NH_2-coated nanoparticles the surface charge is more positive, due to the presence of protonated amine groups (NH_3^+) at the surface. Despite still having some $Si\text{-}O^-$ groups, which contributes to the overall negative charge. After functionalization with acryloyl chloride, NH_3^+ groups react and form an amide bond rendering an -ene group with no charge. As expected, since we are eliminating the contribution of the positively charged groups, after the functionalization, the zeta potential decreases which is indicative of a successful functionalization. As expected, after DNA immobilization, the zeta potential decreased (-38.20 mV) due to the addition of several phosphate groups presented in the DNA probe, thus contributing to an increase of the surface negative charge.

It is important to mention that throughout all the process (from the POM to the core-shell nanoparticles functionalized with DNA) the EuW_{10} compounds were able to maintain their fluorescence when excited under a UV lamp with radiation of 254 nm, as it is shown in Figure 31. As mentioned above, the $EuPW_{11}$ could not be excited under the UV radiation of the lamp (254 nm); since our objective was the development of a system with immediate and visible response, we chose to focus on the EuW_{10} core-shell nanoparticles. Figure 32 shows a schematic representation of the entire process, from the $EuW_{10}@SiO_2$ nanoparticles to the $EuW_{10}@SiO_2$-DNA nanoparticles.

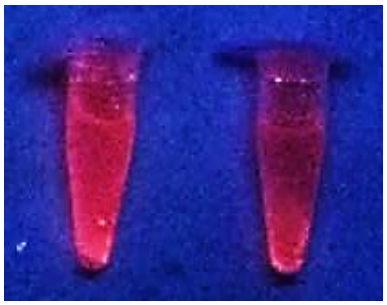

Figure 31: *Aqueous solutions of $EuW_{10}@SiO_2$-NH_2 and $EuW_{10}@SiO_2$-DNA under UV lamp (254 nm)*

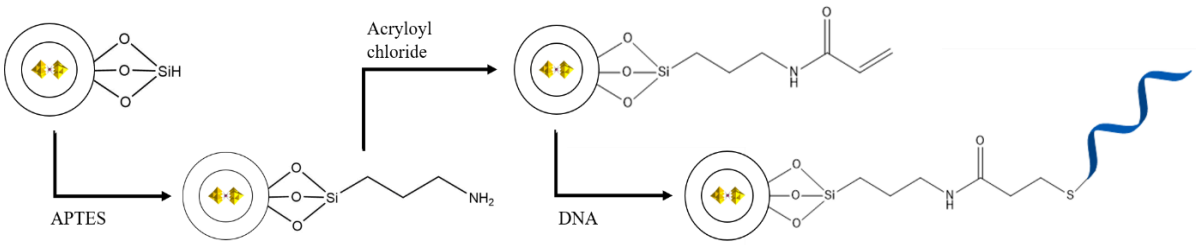

Figure 32: *Schematic representation of the entire process, from the $EuW_{10}@SiO_2$ nanoparticles to the $EuW_{10}@SiO_2$-DNA nanoparticles*

4. DNA detection systems

In this chapter, are described the procedures explored to develop the cellulose-based biosensors, as well as their outcomes and conclusions.

4.1. Capture system

The capture system (Figure 33) used for the DNA detection was constituted by three main recognition elements. The first element is a fusion protein CBM64-ZZ (25.2 kDa) that is constituted by carbohydrate binding module, which binds specifically to cellulose fibrils, and a ZZ fragment able to recognize antibodies via their Fc portion. The second element is an anti-biotin antibody purchased from Abcam, which is anchored onto the paper via CBM64-ZZ interaction (this interaction allows the material to be washed without losing the antibody). The last element is a 5´ biotin-labelled DNA probe, which is recognised by the antibody and allows the capture the target nanoparticles via DNA hybridization. The probe has the following sequence:

biot_5´-ctc tcc gag aac agg cct cga ctt caa-3´

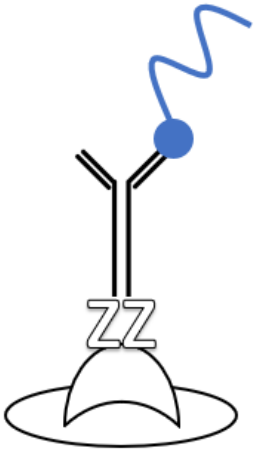

Figure 33: *Minimalist representation of the capture system: CBM64:ZZ complex, anti-biotin antibody and 5´ biotin-labelled DNA probe (blue)*

The CBM64-ZZ:anti-biotin antibody conjugate was prepared in an Eppendorf tube by incubating 0.4 μL of CBM64-ZZ, 0.75 μL of antibody and 0.85 μL of trisodium citrate buffer (TST, 50 mM of Tris buffer, pH 7.4; 150 mM of NaCl; 0.05 % Tween 20) for 30 minutes at room temperature. Then, the 5´ biotin-labelled DNA probe is added and the solution is left to incubate for 20 minutes.

4.2. Paper device assays

Due to the fact of being abundant, easy to process, biocompatible and inexpensive, paper nowadays is widely used for the development of practical, disposable and cheap devices as an alternative for health diagnostics, environmental and quality control applications. Here, the μPAD is limited by wax that creates a hydrophobic barrier, allowing the sample to be pushed by capillarity along the hydrophilic matrix without need of using any external force. Additionally, controlling the size of the box, it is possible to adjust the velocity and volume of the sample that will run in the μPAD.

One of the objectives of this thesis was to develop a paper-based biosensor capable of providing the users rapid and unequivocal information. Unfortunately, as it is shown in Figure 34, after applying 10 μL of a TST buffer solution of the EuW_{10}@SiO_2-DNA nanoparticles on the device, the nanoparticles did not flow through the paper, not reaching the control and test zones.

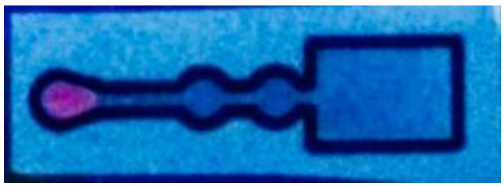

Figure 34: *Application of $EuW_{10}@SiO_2$-DNA nanoparticles on a μPAD*

Electrostatic bonds between the nanoparticles and the paper may be one of the plausible reasons for the failure of this test, so we decided to increase the salt quantity of the TST buffer (from 5 M to 10 M) in order to decrease the interaction between the nanoparticles and the paper. However, as it is shown in Figure 35, the results remained the same. These results indicate that the electrostatic bonds between the paper matrix and the nanoparticles were not the main reason behind the observed lack of flow. The nanoparticles dimensions (not adequately tuned) seem to be the real limiting factor as the TST buffer migrates but the nanoparticles seem to aggregate in the application area.

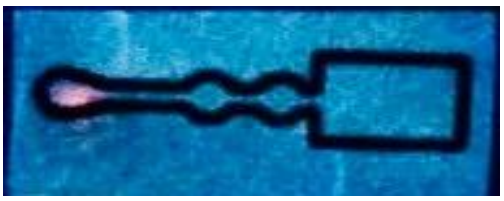

Figure 35: *Application of $EuW_{10}@SiO_2$-DNA on a μPAD (higher concentration of salt)*

4.3. Paper spots assays

An alternative approached was designed where, as for the previous assays, the principle of the biosensor is the attachment of the capture system, although in this case to a delimited area of the paper spot resulting on a well-defined recognition zone.

In this approach, the capture system was applied at the centre of the spot delineated on paper, by wax printing, and dried at room temperature. In a second step, different volumes of a $EuW_{10}@SiO_2$-DNA nanoparticles solution are applied over the same spot

before washing the paper with TST buffer. The observation of the results was made under a UV light lamp with the maximum excitation wavelength at 254 nm.

Our strategy consisted in deposition of the capture system in three different spots. The first one was our test with all the system components, expecting that the fluorescence was maintained only in the area of the capture system deposition; the second one (control 1) was performed with $EuW_{10}@SiO_2$ nanoparticles without the DNA functionalization, expecting that the spot would lose all the fluorescence due to the lack of the target probe – proving the successful DNA hybridization in the first spot; and the last one (control 2) was performed without the 5´ biotin-labelled DNA probe, where, as for the previous test, expecting that the spot would lose all the fluorescence, due to the lack of the recognition element - proving the successful recognition of antibody-antigen in the first spot (Figure 36).

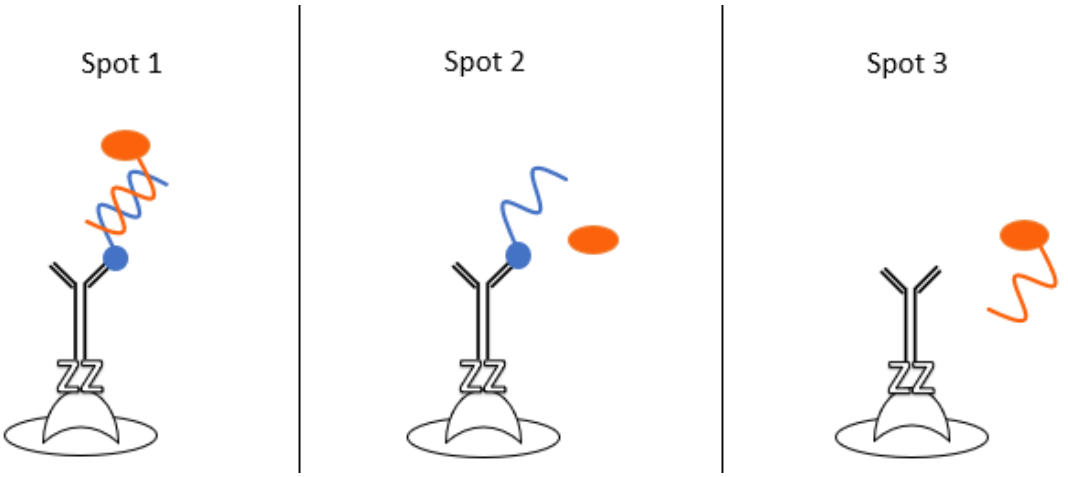

Figure 36: *Representation of the system compounds presented in each spot: CBM64:ZZ complex, anti-biotin antibody, 5´ biotin-labelled DNA probe (blue) and $EuW_{10}@SiO_2$-NH_2 (orange) with or without DNA functionalization*

After the application of the $EuW_{10}@SiO_2$-DNA nanoparticles on the paper surface it is possible to observe a homogeneous distribution of the nanoparticles (which results in an equal distribution of the fluorescence) inside the spots (Figure 37). Figure 38 shows the sensor spots after being washed with TST buffer, and under the UV lamp (254 nm). As expected, the spot 1 retained the fluorescence in the central area, which corresponds to the CBM64-ZZ:anti-biotin antibody conjugate deposition zone. Spots 2 and 3 exhibited the same behaviour, contrary to what was expected. Similarly, to what happened in the µPAD

experiments, the nanoparticles seem to be trapped in the cellulose matrix, retaining them where they are applied, which prevents the wash of the nanoparticles who are not hybridized. It is important to mention that the observed difference between the fluorescence intensity of spot 2 and the others is due to the impossibility to weight the mass of the nanoparticles while preparing the solutions.

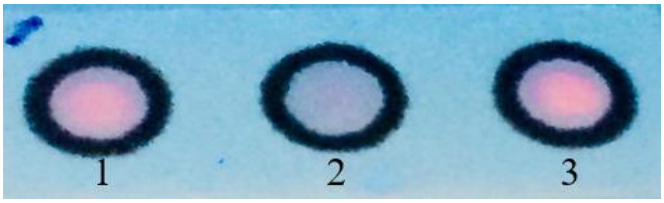

Figure 37: *Paper spots assays before being washed. 1: CBM64-ZZ:anti-biotin antibody conjugate, 5´ biotin-labelled DNA probe and EuW_{10}@SiO_2-DNA nanoparticles; 2: CBM64-ZZ:anti-biotin antibody conjugate, 5´ biotin-labelled DNA probe and EuW_{10}@SiO_2-NH_2 nanoparticles; 3: CBM64-ZZ:anti-biotin antibody conjugate and EuW_{10}@SiO_2-DNA nanoparticles under UV lamp (254 nm)*

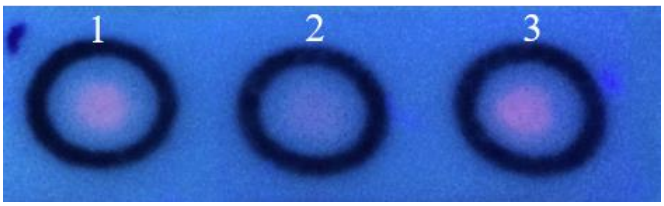

Figure 38: *Paper spots of Figure 34 after being washed with TST buffer under UV lamp (254 nm)*

4.4. Cellulose microparticles assays

Due to the failure of the previous approaches, a “plan C” was elaborated. Herein the principle of the biosensor is similar to the previous test, although in this case the cellulose microparticles (20 μm) are small and dispersed in solution, which can avoid EuW_{10}@SiO_2-DNA nanoparticles to be trapped inside the cellulose matrix.

In this approach, 50 μL of cellulose microparticles (Sigmacell cellulose, type 20, 20 μm) suspended in 1.0 mL of TST buffer (20 mg/mL) were added to each Eppendorf tube. Then, 2 μL of the CBM64-ZZ:anti-biotin antibody conjugate was added to the microparticle suspension and this was incubated for 30 minutes. After the incubation time, a 0.5 μL of biot-DNA (10 μM) was added and the suspension was stirred and incubated for 20 minutes.

Finally, different volumes of the $EuW_{10}@SiO_2$-DNA nanoparticles solution were added, and the suspension was stirred and incubated for 20 minutes. The observation of the results was made under a UV light chamber with the maximum excitation wavelength at 254 nm.

The premise behind these assays was that cellulose particles were the only ones being able to separate from the solution using a simple spinner and the $EuW_{10}@SiO_2$-DNA nanoparticles that do not hybridize with the biot-DNA in the cellulose particles would stay in solution. In Figure 39, it is possible to see the fluorescence in the cellulose microparticles after their deposition. However, the Eppendorf tubes 1 and 2, corresponding to the duplicate sample with the lowest concentration of $EuW_{10}@SiO_2$-DNA nanoparticles did not exhibit any fluorescence, probably because of the low nanoparticles' concentration. So, this assay was repeated with a more concentrated solution of $EuW_{10}@SiO_2$-DNA nanoparticles and a control (without biot-DNA). Tables 1 and 2 show the composition of each tube.

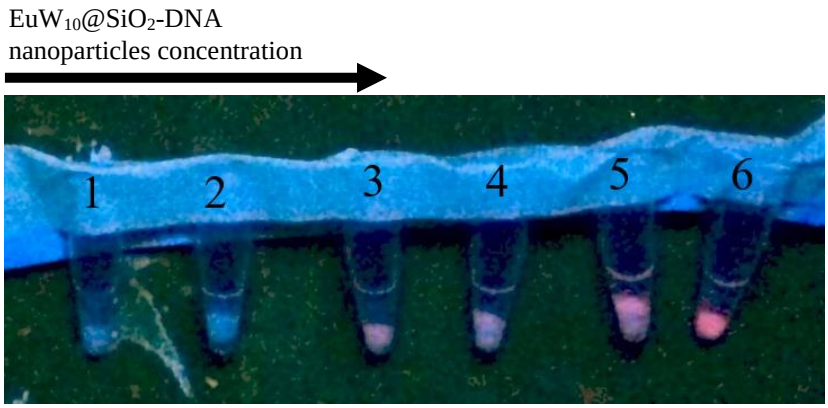

Figure 39: *Cellulose microparticles assays*

In Figure 40, is possible to observe that the cellulose microparticles were able to capture the $EuW_{10}@SiO_2$-DNA nanoparticles (via DNA hybridization) while the C tube only exhibited fluorescence in the supernatant. indicating that our system was functional. As for the previous assay, this was performed with duplicates and with a gradual increase of the concentration of $EuW_{10}@SiO_2$-DNA nanoparticles. Tubes 1 and 2, corresponding to the lowest concentration of nanoparticles used, were the duplicate that showed better "performance", since a very significant difference between the fluorescence intensity of the cellulose microparticles pellet and the supernatant was observed. Fluorescence microplate assays could be done to further evaluate the observed behaviour and to validate this positive,

unfortunately the equipment available was not working. An alternative experiment to overcome this instrumental limitation is to recover the supernatant of each tube and to measure the fluorescence spectra. If differences in the relative intensity of the three main Eu^{3+} transitions (592, 619 and 700 nm) are observed, our system will be validated.

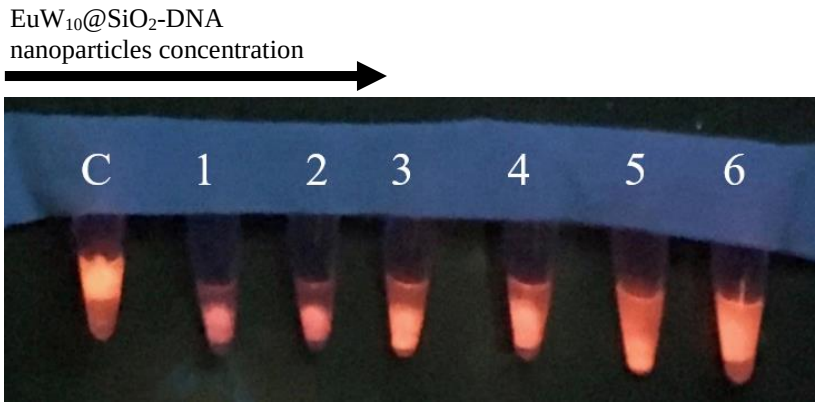

Figure 40: *Cellulose microparticles assays (higher concentration of $EuW_{10}@SiO_2$-DNA nanoparticles). C: control without the biot-DNA*

Table 1: *Summary table of the different volumes of $EuW_{10}@SiO_2$-DNA nanoparticles solution added to each Eppendorf tube used in the cellulose microparticles assay: CBM64:ZZ ($2x10^{-5}$ µmol), Anti-biotin antibody ($5x10^{-5}$ µmol), biot-DNA ($5x10^{-6}$ µmol)*

	1	2	3	4	5	6
$EuW_{10}@SiO_2$-DNA nanoparticles solution (µL)	5	5	15	15	30	30

Table 2: *Summary table of the different volumes of $EuW_{10}@SiO_2$-DNA nanoparticles solution added to each Eppendorf tube used in the cellulose microparticles assay: CBM64:ZZ ($2x10^{-5}$ µmol), Anti-biotin antibody ($5x10^{-5}$ µmol) - higher concentration of $EuW_{10}@SiO_2$-DNA nanoparticles solution*

	C	1	2	3	4	5	6
biot-DNA (µmol)	0	$5x10^{-6}$	$5x10^{-6}$	$5x10^{-6}$	$5x10^{-6}$	$5x10^{-6}$	$5x10^{-6}$
$EuW_{10}@SiO_2$-DNA nanoparticles solution (µL)	30	5	5	15	15	30	30

5. Conclusions

The development of paper-based sensors is considered a subject of most importance due to their promising applications in the areas of clinical diagnostics, environmental monitoring and food quality control. Their main advantages are the low cost and simple fabrication, combined with the fact that they are disposable and easy to transport [103]. With this in mind, this thesis purpose was to fabricate a simple and cost-effective fluorescent paper device for the DNA recognition.

In the case of anion $[EuPW_{11}O_{39}(H_2O)_2]^{4-}$, due to the lack of a suitable UV lamp for adequate excitation, a straightforward strategy was designed to investigate the potential affinity of this anion to interact with DNA. Unfortunately, no notable differences were observed in the fluorescence intensity of the Eu^{3+} transition bands, after the addition of different DNA concentrations, this fact might be due to the low accessibility to the phosphate groups of DNA.

Microemulsion methods, based on the hydrolysis and condensation of TEOS, were used to encapsulate the anion $[Eu(W_5O_{18})_2]^{9-}$ in a silica shell and further functionalizations were performed to immobilize DNA probes onto the nanoparticles´ surface. A detection system was designed to capture target DNA, which relies in biotin labelling of the target.

The molecular detection system was evaluated using a μPAD. In this case, the capture system was applied in the control and test zones (C and T zones) and the $EuW_{10}@SiO_2$-DNA nanoparticles were applied in the sample loading area. The migration of the target system ($EuW_{10}@SiO_2$-DNA) to the C and T zones was not observed, probably due to their aggregation at the paper's surface. Spot assays were also performed to test the capacity of the system to detect DNA. In the assays, CBM64-ZZ:anti-biotin antibody conjugate was immobilized on the paper to capture the $EuW_{10}@SiO_2$-DNA nanoparticles. The results obtained were not the expected as 2 spots used as controls also exhibited luminescence, indicating a possible entrapment of the $EuW_{10}@SiO_2$-DNA nanoparticles in the cellulose matrix.

After these failures, an alternative approach based on the use of cellulose microparticles was explored. In this approach the CBM64-ZZ:anti-biotin antibody conjugate was added to a microparticle suspension. After incubation, the recognition element (biot-DNA) was added and the mixture was further incubated before the addition of the $EuW_{10}@SiO_2$-DNA nanoparticles. Following the addition of nanoparticles and incubation, using a spinner, the deposition of the cellulose microparticles occurred. It was possible to observe that the pellet showed an overall increased luminescence, indicating that the system is functional. Moreover, the fact that in the control, without biot-DNA, the cellulose pellet showed low luminescence corroborates the principle that only the $EuW_{10}@SiO_2$-DNA nanoparticles that had been captured (via hybridization) would deposit after spinning.

In terms of future work, a key challenge will be to optimize the encapsulation process to allow a size tuning, thus avoiding the agglomeration without compromising the fluorescence. If not possible, the encapsulation with polymers, such as alginate, chitosan and styrene, among others should be taken into account. The functionalization should also be optimized by increasing the concentration of DNA per nanoparticle blocking eventual free -ene groups with cysteine or a different molecule containing a thiol group. As the cellulose microparticles test seems to be promising, efforts should be done towards the optimization of this approach regarding the concentration of $EuW_{10}@SiO_2$-DNA nanoparticles in solution and the determination of the biot-DNA working range.

References

[1] Pope, M.T., Müller A. (1991). *Angew. Chem.*, 103, 56-70

[2] López, X., Carbó, J.J., Bo, C., Poblet, J.M. (2012). *Chem. Soc. Rev.*, 41, 7537-7571

[3] Borrás-Almenar, J.J., Coronado, E., Pope, M.T. (2003). *Kluwer Academic Publishers*, Dordrecht

[4] Pope, M. T. (1983). *Springer-Verlag*, Berlin

[5] Volkmer, D., Du Chesne, A., Kurth, D. G., Schnablegger, H., Lehmann, P., Koop, M.J., Müller, A. (2000). *J. Am. Chem. Soc.*, 122, 1995

[6] Polarz, S., Smarsly, B., Göltner, C., Antonietti, M. (2000). *Adv. Mater.*, 12, 1503

[7] Liu, T. (2002). *J. Am. Chem. Soc.*, 124, 10942

[8] Liu, T., Diemann, E., Li, H., Dress, A., Müller, A. (2003). *Nature*, 426, 59

[9] Anyushin, A.V., Smolentsev, A.I., Mainichev, D.A., Vicent, C., Gushchin, A.L., Sokolov, M.N., Fedin, V.P. (2014). *Chem. Commun.*, 50, 9083-9085

[10] Baker, L.C.W., Figgis, J.S. (1970). *J. Am. Chem.*, 92, (12), 3794-3797

[11] Ueda, T., Nishimoto, Y., Saito, R., Ohnishi, M., Nambu, J.I. (2015). *Inorganics*, 3, 355-369

[12] Wu, H. (1920). *J. Biol. Chem.*, 43, (1), 189-220

[13] Baker, L.C.W., Glick, D.C. (1998). *Chem. Rev.*, 98, (1), 3-50

[14] Contant, R., Thouvenot, R. (1993). *Inorg. Chim. Acta*, 212, (1-2), 41-50

[15] Müller, A., Krickemeyer, E., Meyer, J., Bögge, H., Peters, F., Plass, W., Diemann, E., Dillinger, S., Nonnenbruch, F., Randerath, M., Menke, C. (1995). *Angew. Chem.*, 2293–2295

[16] Passadis, S., Kabanos, T.A., Song, Y.F., Miras, H.N. (2018). *Inorganics*, 6, 71

[17] Müller, A., Krickemeyer, E., Bögge, H., Schmidtmann, M., Peters, F. (1998). *Angew. Chem.*, 110, 3567–3571

[18] Floquet, S., Terazzi, E., Hijazi, A., Guénée, L., Piguet, C., Cadot, E. (2012). *New J. Chem.*, 36, 865–868

[19] Peacock, R.D., Weakley, J. R. (1971). *J. Chem. Soc. A.*, (11), 1836

[20] Yamase, T., Ozeki, T., Ueda, K. (1993). *Acta Crystallographica Section C*, 49, (9), 1572-1574

[21] Ozeki, T., Tosaka, M., Yamase, T. (1992). *Acta Crystallographica Section C*, 48, (8), 1370-1374

[22] Ozeki, T., Yamase, T. (1994). *Acta Crystallographica Section C*, 50, (3), 327-330

[23] Yamase, T., Ozeki, T., Tosaka, M. (1994). *Acta Crystallographica Section C*, 50, (12), 1849-1852

[24] Ozeki, T., Yamase, T. (1994). *Acta Crystallographica Section B*, 50, (2), 128-134

[25] Sawada, K., Yamase, T. (2002). *Acta Crystallographica Section C*, 58, (11), 149-151

[26] Omwoma, S., Lagat, S.C., Lalah, J.O. (2018). *Journal of Luminescence*, 196, 294–301

[27] Zhang, S.S., Su, H.F., Wang, Z., Wang, X.P., Chen, W.X., Zhao, Q.Q., Tung, C.H., Sun, D., Zheng, L.S. (2018). *Chem. Eur. J.*, 24, (8), 1998-2003

[28] Long, D.L., Ryo, T., Cronin, L. (2010). *Angew. Chem. Int. Ed.*, 49, (10), 1736-1758

[29] Long, D.L., Cronin, L. (2006). *Chemistry - A European Journal*, 12, (14), 3698-3706

[30] Carlos, L.D., Ferreira, R.A.S., Bermudez, V.Z., Ribeiro, S.J.L. (2009). *Adv. Mater.*, 21, (5), 509-534

[31] Neves, C.S., Granadeiro, C.M., Cunha-Silva, L., Ananias, D., Gago, S., Feio, G., Carvalho, P.A., Eaton, P., Balula, S.S., Pereira, E. (2013). *European Journal of Inorganic Chemistry*, 16, 2877

[32] Qi, W., Li, H., Wu, Li. (2007). *Advanced Materials*, 19, 1983

[33] Mialane, P., Lisnard, L., Mallard, A., Marrot, J., Antic-Fidancev, E., Aschehoug, P., Vivien, D., Sécheresse, F. (2003). *Inorganic Chemistry*, 42, 6

[34] Luong, T.K.N., Mihaylov, T., Absillis, G., Shestakova, P., Pierloot, K., Parac-Vogt, T.N. (2016). *Inorg. Chem., 55* (19), 9898–9911

[35] Feng, J.H., Sun, G.Y., Pei, F.K., Liu, M.L. (2002). *J. Inorg. Biochem.*, 92, (3-4), 193-199

[36] Cécile, B., Gilles, L., Bernold, H., Serge, T., Emmanuel, L., Max, M. (2006). *Angew. Chem. Int. Ed.*,45, (20), 3324-3327

[37] Bünzli, J.C.G., Eliseeva, S.V. (2011). Basics of Lanthanide Photophysics. In *Lanthanide Luminescence: Photophysical, Analytical and Biological Aspects*, 7

[38] Granadeiro, C.M. (2010). PhD Thesis, Universidade de Aveiro

[39] Lehn, J.M., (1990). *Angew. Chem. Int. Ed.*, 29, (11), 1304-1319

[40] Weissman, S.I., (1942). *J. Chem. Phys.*, 10, (4), 214-217

[41] Ferreira, R.A.S., Nobre, S.S., Granadeiro, C.M., Nogueira, H.I.S., Carlos, L.D., Malta, O.L. (2006). *J. Lumin*., 121, (2), 561-567

[42] Yamase, T. (1998). *Chem. Rev.*, 98, (1), 307-326

[43] Granadeiro, C., Ferreira, R.A.S., Soares-Santos, P.C.R., Carlos, L.D., Trindade, T., Nogueira, H.I.S. (2010). *J. Mater. Chem.*, 20, 3313–3318

[44] Ye, Z.Q., Tan, M.Q., Wang, G.L., Yuan, J.L. (2004). *J. Mater. Chem.*, 14, (5), 851-856

[45] Bumb, A., Brechbiel, M.W., Choyke, P.L., Fugger, L., Eggeman, A., Prabhakaran, D., Hutchinson J., Dobson, P.J. (2008). *Nanotechnology*, 19, 335601

[46] Zhang, H., Xu, Y., Yang, W., Li, Q. (2007). *Chem. Mater.*, 19, 5875

[47] Bottini, M., D'Annibale, F., Magrini, A., Cerignoli, F., Arimura, Y., Dawson, M.I., Bergamaschi, E., Rosato, N., Bergamaschi, A., Mustelin, T. (2007). *International Journal of Nanomedicine*, 2, (2), 227–233

[48] Stroobants, K., Moelants, E., Proost, P., Bartik, K., Parac-Vogt, T.N. (2013). *Chem. Eur. J.*, 19, (8), 2848-58

[49] Goovaerts, V., Stroobants, K., Absillis, G., Parac-Vogt, T.N. (2013). *Phys.Chem. Chem. Phys.*, 15, 18378

[50] Liu, J., Mei, W.J., Xu, A.W., Tan, C.P., Shi, S., Ji, L.N. (2004). *Antiviral Research*, 62, 65–71

[51] Bijelic, A., Aureliano M., Rompel, A. (2018). *Chem. Commun.*, 54, 1153-1169

[52] Boulmier, A., Feng, X., Oms, O., Mialane, P., Rivière, E., Shin, C.J., Yao, J., Kubo, T., Furuta, T., Oldfield, E., Dolbecq, A. (2017). *Inorg. Chem.*, 56, (13),7558-7565

[53] Fernández, J. A., Lopez, X., Bo, C., de Graaf, C., Baerends, E.J., Poblet, J.M. (2007). *J. Am. Chem. Soc.*, 129, 12244-12253

[54] Blonder, R., Levi, S., Tao, G., Ben-Dov, I., Willner, J. (1997). *J. Am. Chem. Soc.*, 119, 467- 478

[55] Blonder, R., Ben-Dov, I., Dagana, A., Willner, I., Zisman, E. (1997). *Biosens. Bioelectron.*, 12, 627-644

[56] Prummond, T.G. (2003). *Nature Biotechnol.*, 21, 1192-1199

[57] Wang, J., Rivas, G., Cai, X., Florenda, V., Peter, E.N., *et al*. (1997). *Analytica Chimica Acta*, 347, 1-8

[58] Bagni, G., Osella, D., Sturchio, E., Mascini, M. (2006). *Anal. Chim. Acta*, 574, 81-89

[59] Chikashi, N., Teruaki, K., Masato, M., Makoto, S. (2001). *Molecular Crystals and Liquid Crystals*, 371, 369-374

[60] Arora, K., Prabhakar, N., Chand, S., Malhotra, B. D. (2007). *Biosens. Bioelectronics*, 23, 613-620

[61] Prabhakar, N., Arora, K., Singh, S.P., Pandey, M.K., Singh, H., et al. (2007). *Anal. Chim. Acta*, 589, 6-13

[62] Berdat, D., Marin, A., Herrera, F., Gijs, M.A.M. (2006). *Sensors Actuators*, 118, 53-59

[63] Moina, C., Ybarra, G. (2012). Fundamentals and Applications of Immunosensors. In *Advances in Immunoassay Technology*, 66

[64] Berney, H., West, J., Haefele, H., Alderman, J., Lane, W., *et al.* (2000). *Sens Actuators*, 68, 100-108

[65] Erdem, A., Kesman, K., Mesie, B., Akarea, U.S., Osoz, M., (2000). *Anal. Chim. Acta*, 423, 139-149

[66] Campbell, C.N., Gal, D., Cristler, N., Banditrat, C., Heller, A. (2002). *Anal. Chem.*, 74, 158-162

[67] Millan, K.M., Mikkelsen, S. R. (1993). *Anal. Chem.*, 65, 2317-2324

[68] Malhotra, B.D., Chaube, A. (2003). *Sens. Actuators B Chem.*, 91, 117–126

[69] Annelies, B., Dirk, B., Michel, L. (2005). *Point Care*, 4, 36–40

[70] Kavita, V. (2017). *J Bioengineer & Biomedical Sci.*, 7, 2

[71] Conroy, P.J., Hearty, S., Leonard, P., O'Kennedy, R.J. (2009). *Semin. Cell Dev. Biol.*, 20, 10–26

[72] Kierny, M.R., Cunningham, T.D., Kay, B.K. (2012). *Nano.Rev.*, 3, 17240

[73] Palazon, F., Benavides, C.M., Léonard, D., Souteyrand, E., Chevolot, Y., Cloarec, J.P. (2014). *Langmuir*, 30, 4545−4550

[74] Herman, B. (1998). Fluorescence Microscopy. *2nd ed. Springer-Verlag New York Inc.*, 170

[75] Boisen, M.L., Oottamasathien, D., Jones, A.B., Millett, M.M., Nelson, D.S., Bornholdt, Z.A., *et al.* (2015). *J. Infect. Dis.* 212 (Suppl. 2), S359–367

[76] Nielsen, K., Yu, W.L., Kelly, L., Bermudez, R., Renteria, T., Dajer, A., *et al.* (2008). *J. Immunoassay Immunochem*. 29, 10–18

[77] Rohrman, B.A., Leautaud, V., Molyneux, E., Richards–Kortum, R.R. (2012). *PLoS One,* 7, e45611

[78] Kamphee, H., Chaiprasert, A., Prammananan, T., Wiriyachaiporn, N., Kanchanatavee, A., Dharakul, T. (2015). *PLos One*, 10, e0137791

[79] Koczula, K.M., Gallotta, A. (2016). *Essays in Biochemistry*, 60, 111–120

[80] Nazaré, M.R. (2016). Master´s Thesis, Instituto Superior Técnico

[81] Bahadir, E.B., Sezginturk, M.K. (2016). *Trends in Analytical Chemistry*, 82, 286–306

[82] Majdinasab, M., Sheikh-Zeinoddin, M., Soleimanian-Zad, S., *et al.* (2015). *J. Chromatogr. B*, 974, 147–154

[83] Zhan, F., Wang, T., Iradukunda, L., Zhan, J. (2018). *Analytica Chimica Acta*, 1036, 153-161

[84] Takalkar, S., Baryeh, K., Liu, G. (2017). *Biosensors and Bioelectronics*, 98, 147–154

[85] Sapountzi, E., Tragoulias, S., Kalogianni, D., Ioannou, P., Christopoulos, T. (2015). *Analytica Chimica Acta*, 864, 48–54

[86] Bamrungsap, S., Apiwat, C., Chantima, W., Dharakul, T., Wiriyachaiporn, N. (2014). *Microchim Acta*. 181, 223–230

[87] Fung, K.K., Chan, C.P.Y., Renneberg, R. (2009). *Analytica Chimica Acta*, 634 89–95

[88] Kavosi, B., Hallaj, R., Teymourian, H., Salimi, A. (2014). *Biosensors and Bioelectronics*. 59, 389–396

[89] Yang, W., Li, X., Liu, G., Zhang, B., Zhang Y., Kong, T., Tang, J., Li, D., Wang, Z. (2011). *Biosensors and Bioelectronics*. 26, 3710–3713

[90] Anfossi, L., Di Nardo, F., Giovannoli, C., Passini, C., Baggiani, C. (2013). *Anal Bioanal Chem.* 405, 9859–9867

[91] Posthuma-Trumpie, G.A., Wichers, J.H., Koets, M., Berendsen L.B.J.M., Amerongen, A. (2012). *Anal Bioanal Chem.* 402, 593–600

[92] Jaiswal, J.K., Simon, S.M. (2004). *Trends in Cell Biology.* 14, 497-504

[93] Costa-Fernández, J.M., Pereiro, R., Sanz-Medel, A. (2006). *Trends in Analytical Chemistry*, 25, 207-218

[94] Shiohara, A., Hoshino, A., Hanaki, K., Suzuki, K., Yamamoto, K., (2004). *Microbiology and Immunology*, 48, 669-675

[95] Tan, W., Wang, K., He, X., Zhao, X.J., Drake, T., Wang, L., Bagwe, R.P. (2004). *Med Res Rev*, 24, 621–638

[96] Santra, S., Zhang, P., Wang, K., *et al.* (2001). *Anal Chem*, 73, 4988–4993

[97] Smith, J.E., Medley, C.D., Tang, Z., Shangguan, D., Lofton, C., Tan, W. (2007). *Anal Chem*, 79, 3075–3082

[98] Haraguchi, N., Okaue, Y., Isobe, T., *et al*. (1994). *Inorg. Chem.* 33, 1015-1020

[99] Huang, W., Schopfer, M., Zhang, C., Howell, R.C., Gee, B.A., Francesconi, L.C., Polenova, T. (2006). *J. Phys. Chem. B, 110*, 12340-12350

[100] Jiang, M., Liu, M. (2007). *Journal of Colloid and Interface Science*, 316 100–106

[101] Lavinia, G., Boda, F., Gaz-Florea, A.S., Curticăpean, A., Muntean, D.L. (2014). *Acta Medica Marisiensis*, 60, 84-88

[102] Liu, Y., Hou, W., Sun, H., Cui, C., Zhang, L., Jiang, Y., *et al*. (2017). *Chem. Sci.*, 8, 6182–6187

[103] Rosa, A.M.M., Louro, A.F., Martins, S.A.M., Inácio, J., Azevedo, A.M., Prazeres, D.M.F. (2014). *Anal. Chem.*, 86, 4340−4347